Experimental Neurology 322 (2019) 113063

Contents lists available at ScienceDirect

Experimental Neurology

journal homepage: www.elsevier.com/locate/yexnr

Research paper

Amelioration of visual deficits and visual system pathology after mild TBI via the cannabinoid Type-2 receptor inverse agonism of raloxifene

Marcia G. Honig[a], Nobel A. Del Mar[a], Desmond L. Henderson[a], Tyler D. Ragsdale[a], John B. Doty[a], Jake H. Driver[a], Chunyan Li[a], Andrew P. Fortugno[a], William M. Mitchell[a], Aaron M. Perry[a], Bob M. Moore[c], Anton Reiner[a,b,*]

[a] Department of Anatomy and Neurobiology, The University of Tennessee Health Science Center, Memphis, TN 38163, United States of America
[b] Department of Ophthalmology, The University of Tennessee Health Science Center, Memphis, TN 38163, United States of America
[c] Dept. of Pharmaceutical Sciences, The University of Tennessee Health Science Center, Memphis, TN 38163, United States of America

ARTICLE INFO

Keywords:
TBI
Visual deficits
Microglia
CB2 receptors
Therapy

ABSTRACT

Visual deficits after traumatic brain injury (TBI) are common, but interventions that limit the post-trauma impairments have not been identified. We have found that treatment with the cannabinoid type-2 receptor (CB2) inverse agonist SMM-189 for 2 weeks after closed-head blast TBI greatly attenuates the visual deficits and retinal pathology this otherwise produces in mice, by modulating the deleterious role of microglia in the injury process after trauma. SMM-189, however, has not yet been approved for human use. Raloxifene is an FDA-approved estrogen receptor drug that is used to treat osteoporosis, but it was recently found to also show noteworthy CB2 inverse agonism. In the current studies, we found that a high pressure air blast in the absence of raloxifene treatment yields deficits in visual acuity and contrast sensitivity, reductions in the A-wave and B-wave of the scotopic electroretinogram (ERG), light aversion, and increased pupil constriction to light. Raloxifene delivered daily for two weeks after blast at 5–10 mg/kg mitigates or eliminates these abnormalities (with the higher dose generally more effective). This functional rescue with raloxifene is accompanied by a biasing of microglia from the harmful M1 to the helpful M2 state, and reductions in retinal, optic nerve, and oculomotor nucleus pathology. We also found that raloxifene treatment is still effective even when delayed until 48 h after TBI, and that raloxifene benefit appears attributable to its CB2 inverse agonism rather than its estrogenic actions. Our studies show raloxifene is effective in treating visual injury after brain and/or eye trauma, and they provide basis for phase-2 efficacy testing in human clinical trials.

1. Introduction

Traumatic brain injury (TBI) is a frequent consequence of motor vehicle accidents, falls, and sports activities for the general population, as is exposure to explosive blasts in the case of members of the military. Even mild TBI, with a very brief or no loss of consciousness (i.e. concussion), can produce adverse sensory, motor, cognitive and emotional outcomes. Although resting is often sufficient treatment for symptoms to resolve within a few weeks, some individuals are burdened by persistent problems (Hiploylee et al., 2017). Among these are visual deficits, including impairments in acuity, contrast sensitivity, convergence, accommodation, eye movements, and pupillary constriction, which often result in difficulty reading, double vision, and light aversion (Du et al., 2005; Goodrich et al., 2013; Jacobs and Van Stavern, 2013; Capó-Aponte et al., 2017; Armstrong, 2018). For individuals who experience persisting visual deficits, the use of eyeglasses with specially prescribed tints and prism combinations currently provides the best solution (Armstrong, 2018), as effective treatments for TBI per se are lacking.

As part of a concussive event, whether from sudden impact, acceleration-deceleration, or blast pressure waves, the resulting forces are transmitted across the skull and cause brain tissue compression, stretching, and dynamic shear. Axons are especially vulnerable to deformation, and so damage to the optic nerves, optic radiation and/or cranial oculomotor nerves is frequently observed in people with mild TBI and contributes significantly to their visual deficits (Lachapelle et al., 2004; Bruce et al., 2006; Caeyenberghs et al., 2010; Goodrich et al., 2013; Jacobs and Van Stavern, 2013).

Axonal injury sets off a wave of secondary injury cascades, one of

* Corresponding author at: Department of Anatomy & Neurobiology, University of Tennessee Health Science Center, 855 Monroe Ave, Memphis, TN 38163, United States of America.
E-mail address: areiner@uthsc.edu (A. Reiner).

https://doi.org/10.1016/j.expneurol.2019.113063
Received 3 June 2019; Received in revised form 9 August 2019; Accepted 7 September 2019
Available online 10 September 2019

the more prominent being microglial activation, which in turn causes further damage and worsens the outcome of the initial trauma (Kumar and Loane, 2012; Kumar et al., 2016; Donat et al., 2017). Microglial activation is thus an attractive therapeutic target and drugs acting on activated microglia may provide an effective approach for reducing the injury. Cannabinoid type-2 receptors (CB2) are normally expressed at low levels in the brain, but at higher levels on microglia than on neurons (Ashton and Glass, 2007; Stella, 2010). Activated microglia rapidly increase their expression of CB2 receptors (Ashton and Glass, 2007; Stella, 2010; Schomberg and Olson, 2012; Donat et al., 2014), and so drugs acting on CB2 receptors selectively target microglia (Stella, 2010). CB2 inverse agonists show particular promise (Lunn et al., 2006, 2008). CB2 inverse agonists stabilize CB2 receptors, which are otherwise constitutively active, in an inactive state and reduce adenylyl cyclase inhibition, thereby increasing cyclic adenosine monophosphate (cAMP) production (Atwood et al., 2012). This in turn leads to downstream activation of protein kinase A, which phosphorylates the cAMP response element binding protein (CREB). The transcriptional activity of phosphorylated-CREB (pCREB) has the overall effect of biasing activated microglia from the pro-inflammatory M1 state toward the protective M2 state, thereby underlying the beneficial effects of CB2 inverse agonists (Lunn et al., 2006, 2008; Presley et al., 2015).

We have previously shown that the selective CB2 inverse agonist SMM-189 reduces the M1 features and increases the M2 features of human and murine microglia in vitro (Presley et al., 2015; Reiner et al., 2015). Moreover, daily treatment of mice with SMM-189 for 2 weeks following focal cranial blast TBI greatly attenuates the visual, motor and emotional deficits, neuron loss, and electrophysiological abnormalities that are typically present at 1–2 months (Heldt et al., 2014; Reiner et al., 2015; Bu et al., 2016; Liu et al., 2017; Guley et al., 2019). As part of our SMM-189 studies, we showed that SMM-189 treatment increases levels of nuclear pCREB and biases microglia toward an M2 state in vivo (Bu et al., 2016; Guley et al., 2019), and that the 2-week SMM-189 treatment regimen rescues contrast sensitivity deficits, optic nerve axon loss, and retinal pathologies the mice would otherwise exhibit a month after TBI (Guley et al., 2019). SMM-189, however, is an experimental drug that has not been approved for human use. By contrast, raloxifene, which was recently found to have noteworthy CB2 receptor inverse agonism (Kumar and Song, 2013), is already approved by the Food and Drug Administration (FDA), though due to its action as a selective estrogen receptor modulator. Given that raloxifene is proven safe for human use, if shown to be effective in animal models of TBI, it could be fast-tracked for repurposing as a TBI therapy. Here we sought to evaluate the benefit of raloxifene for mitigating several visual deficits and the associated visual system pathology after mild TBI using our focal blast mouse model and to examine how raloxifene treatment affects microglia in the retina, optic nerve, and brain.

2. Methods

2.1. Animals, TBI and drugs

2.1.1. Animals

Male C57BL/6 mice (Jackson Laboratories, Bar Harbor, ME) received either 50-psi or sham blast at about 3 months of age, and they were then injected over the next two weeks with either raloxifene or vehicle. A series of functional tests were administered to the mice beginning at 30 days after blast. Mice were typically perfused at ~ 8 months post-blast when functional testing was complete, and the eyes, optic nerves and brains dissected and prepared for histological evaluation. Optic nerves from additional mice, some at ~ 2 months and others at ~ 16 months after injury were also used for axon counts, and included in the analysis as we found that axon abundance was not correlated with post-blast survival time or with the age of the animal at sacrifice for any of the experimental groups. A cohort of 15 mice was sacrificed 5 days after blast for histological analysis. Eyes, optic nerves and brains were separately collected from additional small cohorts of mice at 1, 3, and 5 days after blast for qPCR analysis. All experiments were performed in compliance with the Association for Research in Vision and Ophthalmology (ARVO) statement on the Use of Animals in Ophthalmic and Vision Research, with National Institutes of Health (NIH), Department of Defense (DOD), and The University of Tennessee Health Science Center institutional guidelines, and with institutional and DOD approval.

2.1.2. Blast TBI device and blast administration

Our blast model of mild TBI has been previously described in considerable detail (Guley et al., 2016). In brief, the blast device is a modified, horizontally mounted paintball gun that emits a brief high-pressure air blast calibrated to the desired pressure, in this case 50 pounds per square inch (psi) above atmospheric pressure, to consistently produce a moderate level of injury with nearly 99% survival. Mice were anesthetized with Avertin, placed on a cushioned sling, and then inserted into protective tubing that shielded the mouse, except for a 7.5 mm diameter area halfway between the ear and the eye on the left side of the head. Mice that received a sham (0-psi) blast were handled in the identical way, but with a metal plate inserted between the barrel of the paintball gun and the mouse holder. After blast, mice were kept warm and recovered from the anesthesia in 15–30 min. Tylenol was provided in the drinking water at 35 mg/ml for 24 h before and after blast.

2.1.3. Raloxifene and vehicle administration

Raloxifene was prepared in a vehicle containing ethanol:Cremophor:0.9% saline (5:5:90) and administered at a dose of 5 or 10 mg/kg of body weight. Mice were injected intraperitoneally (ip) with either raloxifene or vehicle, beginning at 2 h after blast, and again at approximately the same time every day (± 1 h) for the next 14 days (15 doses in total), unless they were sacrificed at an earlier time point. For brevity, mice that received blast and vehicle will henceforth be referred to as blast-vehicle, sham mice that received vehicle as sham-vehicle or simply sham, mice that received blast and drug as blast-raloxifene, or more specifically blast-raloxifene5 for the lower dose and blast-raloxifene10 for the higher dose.

2.1.4. Additional drugs

To determine if raloxifene benefit stems from its agonist effects on β-type estrogen receptors (ER-β), or its antagonism at α-type estrogen receptors (ER-α) (Habib and Beyer, 2015; Frick et al., 2015), we performed experiments using several drugs that are selective for these two types of estrogen receptors. These were the ER-β antagonist 4-[2-Phenyl-5,7-bis(trifluoromethyl)pyrazolo[1,5-*a*]pyrimidin-3-yl]phenol (PHTPP) (1 mg/kg; Sigma-Aldrich), the selective ER-β agonist 2,3-Bis (4-hydroxyphenyl)propionitrile (DPN) (1 mg/kg; Sigma-Aldrich), and the selective ER-α antagonist 1,3-Bis(4-hydroxyphenyl)-4-methyl-5-[4-(2-piperidinylethoxy)phenol]-1H-pyrazole dihydrochloride hydrate (MPP) (1 mg/kg; Sigma-Aldrich) (Li et al., 2017). The MPP and PHTPP doses were 3-fold greater than those shown to be effective in prior studies (Li et al., 2017), and the DPN dose was the same as or as much as 10-fold greater than the effective dose used in studies by others (Waters et al., 2009; Pisani et al., 2016). In an additional study, to verify that CB2 inverse agonism accounts for the benefit of raloxifene, we administered the selective CB2 inverse agonist SR144528 at 6 mg/kg (Cayman Chemical). In all cases, these drugs were prepared in the same vehicle as raloxifene, the injections were ip, and administration began 2 h after blast and continued for an additional 14 days.

2.2. Functional testing

2.2.1. Contrast sensitivity and visual acuity

The optokinetic reflex was used to determine the contrast sensitivity threshold and visual acuity of mice before and about one month post-

blast, using a Cerebral Mechanics OptoMotry system (CerebralMechanics Inc.: www.cerebralmechanics.com). The test was administered in a double-blinded manner, with the experimenter unaware of both the stimulus presented to the mouse and the eye being tested at any given time, as well as the treatment group. Contrast sensitivity threshold was determined at a 0.042 c/d spatial frequency and visual acuity was assessed at 100% contrast, as in our prior studies (Reiner et al., 2015; Guley et al., 2016, 2019). As there were no significant pre-blast differences between experimental groups for either eye, the post-blast data for the groups were normalized relative to sham pre-blast performance to better evaluate the effect of TBI.

2.2.2. Electroretinogram (ERG)

For full-field ERG recordings, mice were dark adapted for 12 h, anesthetized with ketamine-xylazine, and the pupils dilated with 1% cyclopentolate hydrochloride. A drop of methylcellulose solution (Celluvisc; Allergan, Irvine, CA) was applied to each eye to protect it and help maintain a good electrical connection. Animals were kept on a warm (38 °C) pad during the procedure. Full-field ERGs were recorded from both eyes using the Diagnosys LLC system. Gold wires placed on each eye served as the corneal electrodes, and a steel subdermal needle served as the reference electrode. For grounding, a steel needle was placed in the tail. Animals received the following series of dim flashes to assess the scotopic (rod) A-wave and B-wave responses: 1) 0.00001 cd.*sec*/m^2 (15 trials with a 5 s interstimulus interval, ISI); 2) 0.0001 cd.sec/m^2 (10 trials with a 5 s ISI); 3) 0.001 cd.sec/m^2 (3 trials with a 10.1 s ISI); 4) 0.01 cd.sec/m^2 (3 trials with a 15.1 s ISI); 5) 0.1 cd.sec/m^2 (2 trials with a 20 s ISI); 6) 1 cd.sec/m^2 (2 trials with a 20 s ISI); and 7) 2.88 cd.sec/m^2 (2 trials with a 20 s ISI). Note that there were fewer trials and longer ISIs at the higher light intensities to limit rod photopigment bleaching, which would then affect subsequent trials. We measured the A-wave and B-wave amplitudes before blast and about 6–8 weeks after blast, and normalized data from the different groups relative to sham pre-blast performance to better assess TBI effects. No significant pre-blast differences were found between groups for either eye.

2.2.3. Light/dark testing to assess light aversion

The light-dark test arena consisted of a clear-walled test arena containing two equally sized compartments – an open area surrounded by the clear Plexiglas walls of the overall test arena and an enclosed chamber with black Plexiglas walls. An opening in the latter allowed the mice free passage from one chamber to the other. Infrared laser beams throughout the arena detected mouse movement and location, and a program automatically measured how much time the mouse spent in each compartment. The enclosed chamber contained a light bulb that could provide illumination at 500 lux, 1000 lux or 1500 lux, but was otherwise at 0 lux. The entire test arena was covered by a black drape during the testing, to prevent the mouse from being distracted by room cues or room lighting. The illumination of the open chamber was slightly $>$ 0 lux when draped and ranged from 2 to 10 lux as illumination of the enclosed chamber was increased. Mice, which are nocturnal, tend to spend more time in the enclosed chamber under normal circumstances, as it provides a place the mouse can hide. Mice were habituated to the arena at ~100 days after blast to reduce the anxiety they would have otherwise demonstrated when exposed to a novel environment (Matynia et al., 2012), and tested about a month later. For the test, the mouse was placed in the open side and the arena covered with the drape. Each test began with 5 min of no light in the enclosed chamber (0 lux), followed by 5 min each of 500, 1000 and 1500 lux. As mice are naturally averse to bright light, they spend less time in the enclosed chamber as its illumination increases. Any increased avoidance of the enclosed chamber was interpreted as increased light aversion.

2.2.4. Pupillometry

Pupillometry was carried out under scotopic conditions on awake mice that were held using minimal manual restraint, having been previously habituated by extensive handling. We used a Melan-100 instrument (BioMed Vision Technologies, Ames, IA), equipped with two diode-based light sources: 630 nm for red light (200 kilocandela per square meter, kcd/m^2) and 480 nm for blue light (200 kcd/m^2). Red light elicits pupillary constriction mediated by rods and/or cones, whereas blue light elicits a response attributable to rods/cones and to intrinsically photosensitive retinal ganglion cells (ipRGCs) during light exposure, with the ipRGC response persisting after light offset. Pupil responses were recorded using a digital infrared video camera (Sony Handycam; Sony Corporation). An image of baseline pupil diameter was first taken in the dark. One eye was illuminated at a time, at a distance of 4 cm for 2 s, beginning with the red light, and then after a 10-s recovery period, with the blue light. Five minutes was allowed to elapse before testing the other eye. Frames from the captured movies were analyzed with Image J to measure pupil diameter and area before, during and after the light stimulus.

2.3. Morphological and immunohistochemical studies

2.3.1. Animal sacrifice

Mice were deeply anesthetized (Avertin; 0.2 mL/g body weight), the chest opened, and 0.1 mL of heparinized saline (800 U.S.P. units/mL) injected into the heart. Mice were then perfused transcardially with 30 mL of 0.9% NaCl in 0.1 M sodium phosphate buffer at pH 7.4 (PB), followed by 60 mL of 4% paraformaldehyde, 0.1 M lysine-0.1 M sodium periodate in 0.1 M PB at pH 7.4 (PLP). Brains were removed, and a pin inserted longitudinally into the right side of each brain, so that the left and right sides of the brain could be distinguished after sectioning. The brain was placed in PLP overnight 4 °C to post-fix, and the following day transferred to a 20% sucrose/10% glycerol solution and stored at 4 °C until sectioned. Each eye was removed from its socket, infused with PLP and post-fixed for 2 h at 4 °C. The lens and cornea were then removed. The eye cup was transferred to 0.1 M PB/0.01% sodium azide at 4 °C for storage, while the optic nerve was post-fixed in 4% paraformaldehyde/0.5% glutaraldehyde in 0.1 M PB, for later embedding in plastic.

2.3.2. Tissue sectioning and immunolabeling

Fixed brains were frozen with dry ice and sectioned on a sliding microtome in the transverse plane at 35 μm. Eyes were immunostained as eye cups and prepared as retinal flat-mounts, as described in more detail below. Plastic-embedded optic nerves were sectioned transversely at 1 μm and stained with 1% *p*-phenylenediamine in 50% methanol. Immunohistochemistry on free-floating brain sections was performed by peroxidase-antiperoxidase labeling or by multiple immunofluorescence, as described in our prior studies (Reiner et al., 2015; Guley et al., 2019). Image analysis was performed by individuals blind to treatment group.

2.3.3. Optic nerve axon counts

We viewed optic nerve sections using an Olympus BH2 light microscope with S Plan Apochromat objectives and an achromatic condenser (Olympus Corporation, Tokyo, Japan) and captured images with a SPOT Idea™ camera (Diagnostic instruments, Inc., Sterling Heights, MI), as described previously (Guley et al., 2019). A low-power image of each optic nerve was first captured using a 20x objective to measure its cross-sectional area and to divide the nerve into quadrants. An image of a subfield within each quadrant was then captured near its mid-point, using a 100x oil immersion objective. The image of each subfield was overlain with a 4 × 6 grid of twenty-four 100 μm^2 counting boxes. A random number generator was used to select 2 boxes per row per grid in which to count axons. Axon density was calculated for each quadrant, the densities for the 4 quadrants were averaged, and then the total

number of axons was estimated by multiplying the optic nerve cross sectional area by the axon density.

2.3.4. Analysis of ipRGCs

To help in understanding the basis for changes in light aversion and pupil constriction, we assessed melanopsin expression by intrinsically photosensitive retinal ganglion cells (ipRGCs) using the intensity of immunolabeling as a readout of relative expression levels. To do this, we immunostained eye cups for melanopsin, in combination with s-opsin, and prepared retinal flat-mounts. For s-opsin, we used a rabbit polyclonal antibody (Abcam #81017), raised against a synthetic peptide from the internal region of the human protein. S-opsin immunostaining specifically labels the outer segments of short wavelength cone photoreceptors, which are more abundant in inferior retina than superior retina (Ouk et al., 2016), thereby allowing us to determine the orientation of each retina. For melanopsin, we used a rabbit polyclonal antibody (Abcam #19306), raised against a synthetic peptide corresponding to amino acids 1–19 of the rat protein (Boudard et al., 2009; Benedetto et al., 2017). As this immunogen is the same as that used to generate a rabbit polyclonal antibody sold by Thermo Fisher (#PA1–780: Lin and Peng, 2013) and nearly identical to the immunogen for #UF006 (Advanced Targeting Systems; Hughes et al., 2013; Ouk et al., 2016), albeit with an additional 4 amino acids, we expect that our melanopsin immunolabeling detected M1 and M2 type ipRGCs (Baver et al., 2008; Berson et al., 2010; Lin and Peng, 2013). Note that although both the melanopsin and the s-opsin antibodies were rabbit polyclonals and visualized with the same secondary antibody, melanopsin+ ipRGCs and s-opsin+ outer segments were nonetheless readily distinguishable by their locations in the inner and outer retina, respectively, and by their distinct morphologies.

The immunostained eye cups were mounted onto slides, flattened, and coverslipped and viewed with a Zeiss 710 confocal microscope (LSM 800, Carl Zeiss AG, Oberkochen, Germany). Images were captured with a 10x, 0.45 numerical aperture objective at 0.8x zoom, and a pinhole setting of 2 Airy units, using the tile capture function of the Zen software (Zen Black Version 2.1, Carl Zeiss AG, Oberkochen, Germany) to allow efficient visualization of the entire retinal surface. Laser power and gain were adjusted to optimize image quality and were standardized across all images for each marker. A set of 3–4 z-stacks was acquired at 6 μm intervals through the inner retina, and another set of 5–6 z-stacks through the outer retina. The z-stack inner retina images and the 3 z-stack outer retina images containing the majority of melanopsin + cells were used to generate separate maximum intensity projection images with the Zen software, and exported as tiff files for analysis with Adobe Photoshop and FIJI. Each image of inner retina was rotated in Adobe Photoshop so that the region of densest s-opsin immunostaining was positioned toward the bottom, and the least dense toward the top (Fig. 1A). The melanopsin image was then rotated the same number of degrees.

As melanopsin expression is known to vary along the superior-inferior axis of the retina (Hughes et al., 2013; Ouk et al., 2016), we took the following approach in our analysis. First, we divided the retinas into counting sectors that were consistent from mouse to mouse, by placing a dot in the center of optic nerve head, and drawing a 2400 μm × 2400 μm square centered on that dot in a separate layer of the Photoshop file. We drew horizontal lines at 600 μm above and below the center, so that the counting area was divided into 4 regions: 600–1200 μm superior retina, 0–600 μm superior retina, 0–600 μm inferior retina, 600–1200 μm inferior retina (henceforth called mid-superior, lower superior, upper inferior, mid-inferior, respectively). We circled all the melanopsin+ ipRGCs as shown in Fig. 1B, using the freehand pencil tool in a different Photoshop layer to facilitate later identification. Each cell was then drawn with a fine pencil in another layer in Photoshop to create a mask, with the opacity of the drawing layer set at 20–30% so that the image could still be seen (Fig. 1C, D). The mask and image layers were opened in FIJI, and the masks selected by thresholding. We next directed the Analyze Particles function to the original melanopsin image to obtain cell body area and optical density (OD) for each melanopsin+ cell. To correct for background OD, which varied across the counting areas and between retinas, we made 3 copies of the mask layer, displacing each in a different direction ~2–5 cell diameters away from the measured ipRGC cells, and measured the OD under each displaced mask for each cell. The average of the 3 background measurements was subtracted from the measured cell OD. In the occasional cases in which a displaced mask was positioned over another melanopsin+ cell or one of the relaxing cuts in the retina, so that its OD was not representative of the background adjacent to the cell of interest, that measurement was excluded.

2.3.5. Oculomotor nuclei

To understand the basis of eye movement abnormalities, we immunolabeled brain sections for choline acetyltransferase (ChAT), using a goat polyclonal antibody (Chemicon #AB144) as in prior studies (Deng and Reiner, 2016). Images were captured at a standardized level through the midbrain, the area of the oculomotor nucleus determined for that section using Image J, and ChAT+ perikarya counted.

2.3.6. Microglia in the optic tract

To begin to assess the effect of raloxifene on microglia, we sacrificed a cohort of 15 mice at 5 days after blast for immunofluorescence analysis. We immunostained sections through the brains of these mice for IBA1, to visualize all microglia, in combination with the M1 marker CD16/32, and the M2 marker CD206, using rabbit anti-IBA1 (Wako Chemicals #019–19,741), rat anti-CD16/32 (Abcam #ab25235), goat anti-CD206 (R&D Systems #AF2535), respectively, as in our previous studies (Guley et al., 2019). We directed our attention to the right optic tract, where reactive microglia are abundant during the first week after 50-psi blast (Guley et al., 2016, 2019). Images were captured with the Zeiss 710 confocal microscope, using a 20x, 0.8 numerical aperture objective, a pinhole setting of 2 Airy units, and the tile capture function of the Zen software. Laser power and gain were adjusted to optimize image quality and were standardized across all images for each marker. A set of 3 z-stacks was acquired at 2 μm intervals, used to generate a maximum intensity projection image with the Zen software, and exported as a tiff file for analysis with Adobe Photoshop and FIJI.

We took the following approach in our analysis. First, we outlined the right optic tract using the freehand pencil tool in Photoshop to determine its area and restrict subsequent analysis to this region. Second, we measured the background labeling intensity in 3 small areas without microglia within the optic tract for each channel for each image, and used the channel average to adjust each channel to a background OD level of 10 (1 = black, 255 = white), using the Math function in FIJI. Third, we then measured the overall mean OD within the right optic tract for each channel for each image. Fourth, for each image we thresholded the IBA1 channel to a standard level, and then used the Analyze Particles function in FIJI with a minimum particle size of 100 pixels (17.4 μm^2) to create a mask of the IBA-1 labeling above threshold. The IBA1 mask was then imported back into Photoshop, where the freehand pencil tool was used to separate any small, closely spaced sets of microglial cells that had been incorrectly joined in FIJI. The corrected mask was then reopened in FIJI and that software used to measure the area above threshold and count the number of particles.

2.4. Pharmacological and qPCR studies

2.4.1. ACTOne cell-based cAMP assay

The functional activity of raloxifene and SMM-189 at CB2 receptors was evaluated using the ACTOne cell-based cAMP assay in HEK-CNG + CB2 cells, as described in Presley et al. (2015). In brief, HEK-CNG + CB2 cells (HEK – human embryonic kidney; CNG – cyclic nucleotide-gated) were plated into clear poly-D-lysine coated 96-well plates at 50,000 cells per 100 μL culture medium with 10% serum the

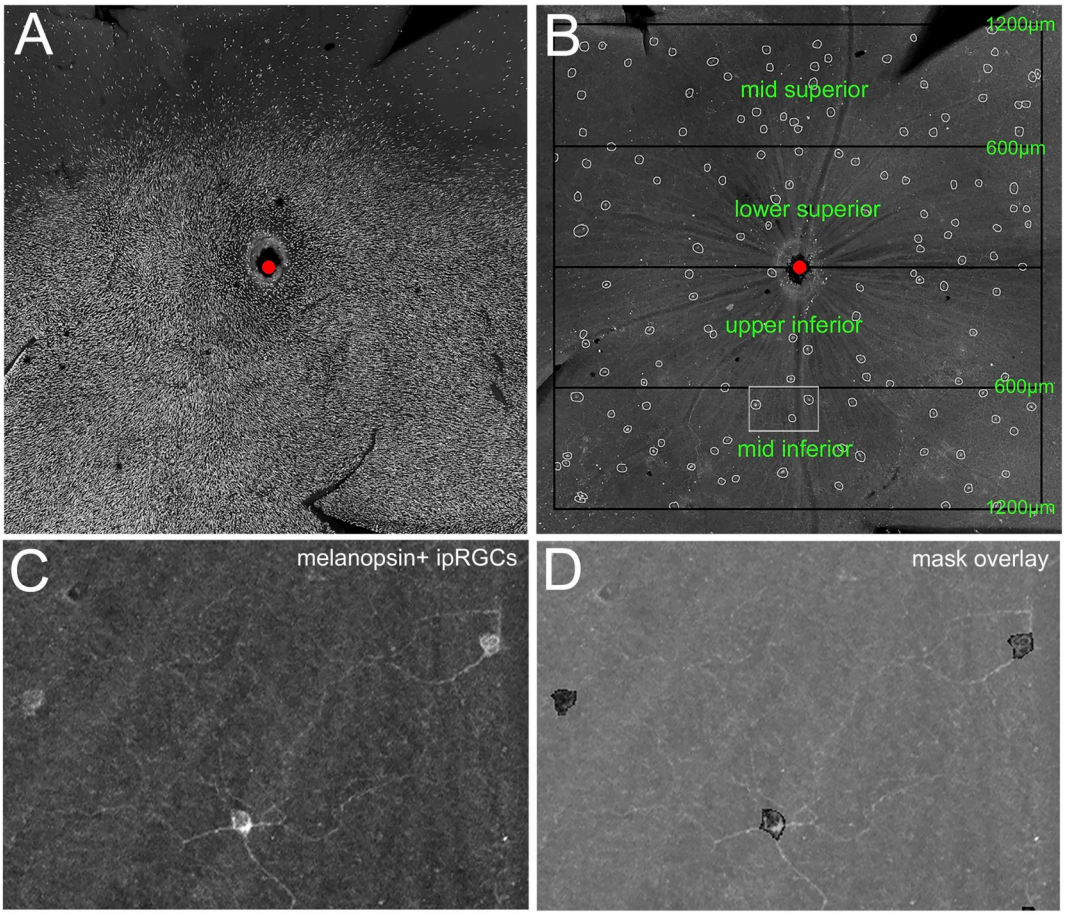

Fig. 1. Approach for analysis of melanopsin+ ipRGCs. **A.** Confocal image of a retinal flat mount showing immunolabeling for S-opsin. The image was rotated to the correct orientation as determined by the high abundance of S-opsin+ outer segments in ventral retina. The location of the optic nerve head is marked by a red dot. **B.** Melanopsin immunolabeling of the same retina shown in A. A 2400 µm × 2400 µm box, centered on the optic nerve head (red dot), was drawn in a separate layer in Photoshop, divided into 4 sectors, and ipRGCs circled for identification. Peripheral retina is beyond the field of view and was not analyzed. **C.** High magnification view of the area marked by the small rectangle in B, showing the labeled cell bodies and processes of three melanopsin+ ipRGCs. **D.** Same field of view as C. Labeled cell bodies were drawn to create a mask to allow measurement of their optical densities. The mask layer is shown overlaid on the image layer at 30% opacity. (For interpretation of the references to colour in this figure legend, the reader is referred to the web version of this article.)

day before experiments were performed. The day of the experiment, 100 µL of warmed ACTOne formulation Membrane Potential Dye was added to each well, and incubated for 1 h in the dark at room temperature. Drug was then added in Dulbecco's phosphate buffered saline (DPBS) with 2.5% (*v*/v) dimethyl sulfoxide (DMSO), with 25 µmol/L Ro 20–1724 (selective inhibitor of cAMP-specific phosphodiesterase), and 800 nmol/L forskolin. Raloxifene and SMM-189 were tested at final concentrations of 10^{-10} to 10^{-5} to span the range from roughly one log unit above and below the previously determined SMM-189 EC50. Plates were read 50 min after raloxifene or SMM-189 addition using a BioTek (Winooski, VT) plate reader (Ex 540 nm, Em 590 nm). At least six biological replicates were used for subsequent data analysis.

2.4.2. qPCR studies

We used quantitative PCR (qPCR) to assess how microglia are modulated by blast TBI and raloxifene treatment. For these studies, the left and right optic nerves, retina, and thalamus were each separately dissected and the tissue homogenized in TRIzol Reagent (Thermo Fisher Scientific, Waltham, MA) following the manufacturer's recommendations. Chloroform was added to the homogenate, centrifuged, and the upper colorless phase transferred to a clean tube. Precipitation was with 100% isopropanol and linear acrylamide. Precipitate was washed with 75% ethanol and the final mRNA pellet was suspended in DEPC (diethylpyrocarbonate) treated water. RNA concentration was assessed by analysis on Qubit Spectrophotometer and RNA purity by a NanoDrop Spectrophotometer. Reverse transcription (RT) was performed using the Transcriptor First Strand cDNA Synthesis Kit (Roche Applied Science, Mannheim, Germany), combining 100 ng of RNA with reaction buffer and enzyme mix, following manufacturer's directions. As it was necessary to linearly amplify the cDNA to produce an adequate amount of cDNA for qPCR from the optic nerve, with its limited volume of tissue and low mRNA harvest, this was done for all tissues using TaqMan® PreAmp Master Mix (Thermo Fisher Scientific, Waltham, MA). To assess the various states of microglia, we used primers for the following transcripts: 1) M0 – ionized calcium-binding adapter molecule 1 (IBA1), transmembrane protein 119 (Tmem119), purinergic receptor P2Y12 (P2ry12), and transforming growth factor-beta (TGFβ); 2) M1 – Fc gamma receptor 2 (CD32), interferon-gamma (IFNγ), interleukin 1-beta (IL1β), tumor necrosis factor-alpha (TNFα), and inducible intric oxide synthase (iNOS); and 3) M2 - Arginase-1 (Arg1), chitinase-like protein 3 (YM1), interleukin-10 (IL10), and triggering receptor expressed on myeloid cells 2 (TREM2). Plates were run using Roche® LightCycler 480 and data were analyzed using the Comparative C_T ($\Delta\Delta C_T$) Method. Primers and probes are shown in Table 1 in the supplementary material. As seven of the thirteen transcripts examined are unique to microglia in these tissues (IBA1, Tmem119, P2ry12, CD16/32, IL1β, Ym1, and TREM2), our data provide evidence on the effects of blast and raloxifene on microglia. While the remaining 6 transcripts are typically considered to be microglial markers, they can also be expressed by astrocytes, oligodendrocytes, and/or neurons. Although the relative

levels of expression of these 6 transcripts for the different cell types in the various tissue sources is not known, it is important to note that there are no neurons in the optic nerve and no oligodendrocytes in the retina.

2.5. Statistical analysis

One-way ANOVA followed by planned comparisons using post-hoc Fisher PLSD (Protected Least Significant Difference) tests was used to analyze behavioral and histological data, unless otherwise stated. Results are presented as group mean ± standard error of the mean (SEM).

3. Results

In the work reported here, we examined the consequences of blast TBI and the benefit provided by raloxifene treatment in terms of visual function and associated morphological changes. Mice were tested for contrast sensitivity and visual acuity at one month after blast, followed by ERGs at ~2 months, light aversion at ~4 months, and pupillometry at ~7 months, before being sacrificed for histological analyses. A few additional subsets of mice were subjected to blast with and without treatment and sacrificed within a few days for immunohistochemical or qPCR analysis to evaluate microglial state.

3.1. Functional benefit of raloxifene

3.1.1. Contrast sensitivity and visual acuity

We have previously reported that a focal blast delivered to the left side of the cranium produces deficits in contrast sensitivity in both eyes (Guley et al., 2016, 2019). In the current series of experiments, as expected, we again found significant increases in contrast sensitivity thresholds for both eyes following blast (Fig. 2A). Contrast sensitivity thresholds for the blast-raloxifene5 mice, however, were significantly lower than in the blast-vehicle mice and similar to the sham mice, both comparisons indicating that contrast sensitivity was improved. The blast-raloxifene10 mice showed a similar pattern of results, with contrast sensitivity thresholds for both eyes restored to a similar level as in sham mice. For this smaller set of animals (10 mice for 10 mg/kg as compared to 22 mice for 5 mg/kg), the improvement in contrast sensitivity compared to blast-vehicle mice was significant for the right eye and trended toward, but did not reach, statistical significance for the left eye. Thus, blast TBI produced bilateral deficits in contrast sensitivity and raloxifene treatment alleviated those deficits.

Optomotor testing of visual acuity for the same animals did not reveal any deficit for the left eye as a consequence of blast. By contrast, visual acuity was significantly reduced for the right eye of blast-vehicle mice compared to sham mice. Visual acuity was improved by both doses of raloxifene, as it was not significantly different than for sham-vehicle mice for both doses, with the blast-raloxifene5 mice also significantly different than the blast-vehicle mice (Fig. 2B).

3.1.2. Scotopic dark-adapted ERG A-wave and B-wave

Scotopic ERGs showed reductions in the peak amplitudes of the A-wave for both eyes and the B-wave for the left eye as a consequence of blast and rescue of these deficits with raloxifene treatment (10 mice per experimental group; Fig. 3). Specifically, the A-wave peak for the 4 brightest light intensities for both eyes was significantly reduced for blast-vehicle mice compared to sham, while blast-raloxifene mice at both doses did not differ from sham. The left eye B-wave peak for the 6 brightest light intensities was also reduced for blast-vehicle mice compared to sham and restored to sham levels in the drug-treated mice. By contrast, the B-wave peak for the right eye did not show significant changes with blast or with drug treatment.

3.1.3. Light aversion

Light aversion was assessed by allowing each mouse to move freely between two chambers, an open chamber kept dark and an enclosed chamber with variable illumination. As shown in Fig. 4, increased illumination in the enclosed chamber resulted in greater avoidance for all groups of mice. The blast-vehicle mice, however, spent significantly less time than sham mice in the increasingly brighter enclosed chamber. Treatment with 10 mg/kg raloxifene rescued this heightened light aversion, as blast-raloxifene10 mice and sham mice occupied the enclosed chamber to similar extents. The blast-raloxifene5 mice, however, still differed significantly from sham. Thus, blast TBI caused light aversion, and the higher dose of raloxifene was needed to prevent this.

3.1.4. Pupil light reflex

To provide insight into the increased light aversion the mice exhibited following blast TBI, we conducted pupillometry. Surprisingly, we found abnormalities in the pupil light reflex (PLR) of the right eye following exposure to red light and to blue light, but not for the left eye (Fig. 5). Pupil constriction for the right eye was significantly enhanced in blast-vehicle mice compared to sham mice, for the 2 s during exposure to red light and during and for up to 10 s after exposure to blue light (Fig. 5B). Treatment with 5 mg/kg raloxifene partly normalized the red light but not the blue light response, whereas 10 mg/kg raloxifene normalized the increased pupil constriction for both red and blue

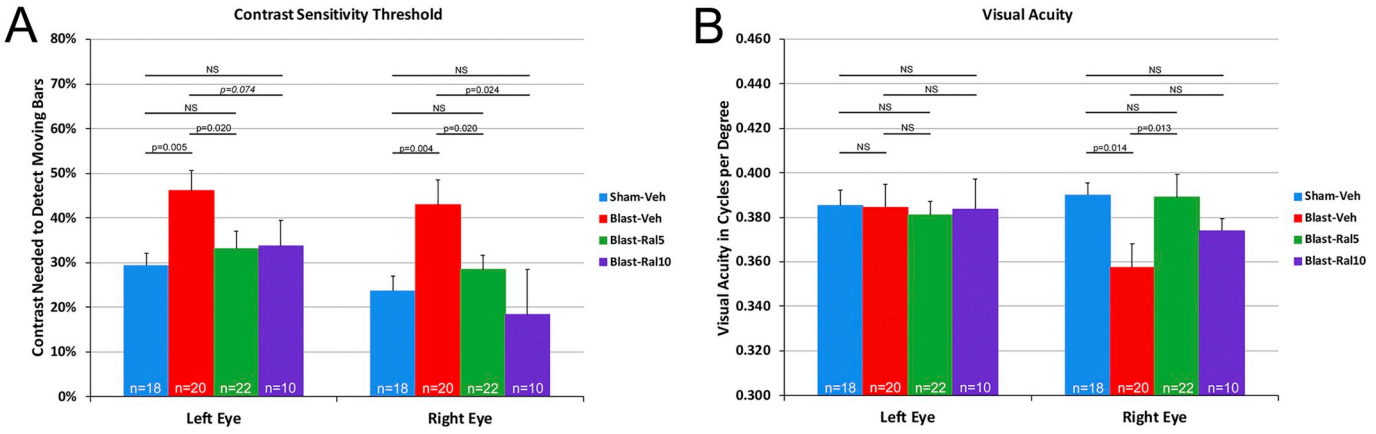

Fig. 2. Contrast sensitivity and visual acuity as measured using Optomotry a month after blast. **A.** The contrast sensitivity thresholds were significantly more in blast-vehicle mice than in sham-vehicle mice for both eyes. Mice treated with raloxifene were similar to sham and improved over blast-vehicle mice, either significantly or in the case of the left eye of the blast-ral10 mice approaching significance. **B.** The right eye of blast-vehicle mice showed a significant loss of acuity compared to sham mice, which was rescued by raloxifene treatment. Acuity for the left eye was similar for the blast-vehicle, blast-raloxifene, and sham mice. N = the number of eyes. Errors bars are SEMs. *p* values that are close to statistical significance are shown italicized.

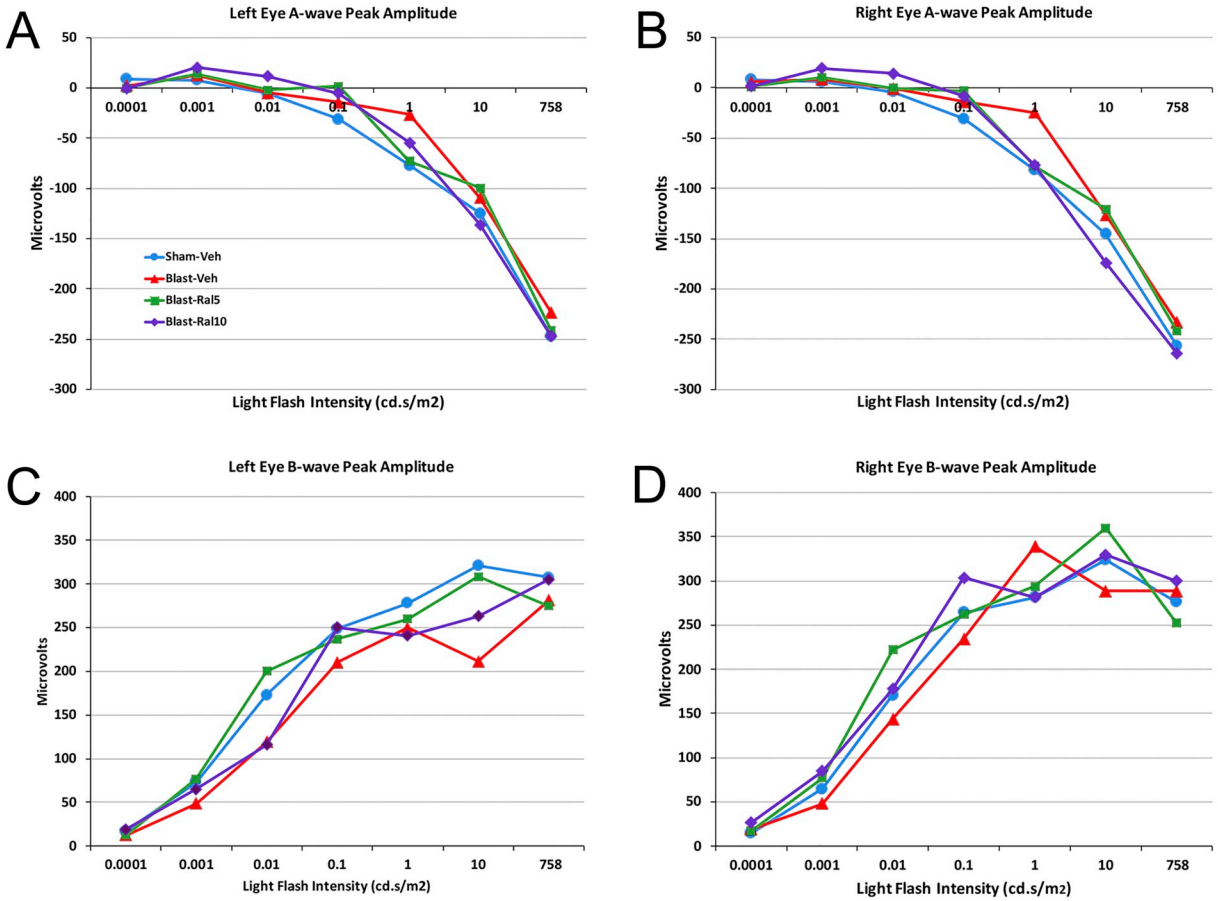

Fig. 3. Average flash-evoked scotopic ERG peak A-wave and B-wave amplitudes at 7 light intensities at ~2 months after blast. Values for each mouse were normalized to the sham pre-blast baseline. **A, B.** The A-wave peak for the 4 brightest light intensities was reduced for blast-vehicle mice compared to sham mice. The reduction for the left eye was significant ($p = .0343$), while blast-raloxifene mice were statistically indistinguishable from sham ($p = .1787$ for blast-raloxifene5 compared to sham, $p = .4664$ for blast-raloxifene10 compared to sham). The right eye showed a similar reduction in the A-wave peak with blast compared to sham ($p = .0251$), and a restoration to sham values in raloxifene-treated mice ($p = .2254$ for blast-raloxifene5 compared to sham; $p = .8602$ for blast-raloxifene10 compared to sham). **C, D.** For the left eye, the B-wave peak, measured from baseline, for the 6 brightest light intensities was reduced for blast-vehicle mice compared to sham mice ($p = .0038$), and blast-raloxifene mice were statistically indistinguishable from sham ($p = .6806$ for blast-raloxifene5 compared to sham; $p = .0867$ for blast-raloxifene10 compared to sham). The B-wave peak for the right eye did not show a significant deficit with blast ($p = .7053$), and blast-raloxifene mice were not significantly different than sham ($p = .3366$ for blast-raloxifene5; $p = .2553$ for blast-raloxifene10).

light (Fig. 5D).

3.2. Morphological benefit of raloxifene

3.2.1. Optic nerve

The left optic nerve of blast-vehicle mice showed a significant 10% loss of axons (Fig. 6). Similar loss was found in the blast mice treated with 5 mg/kg raloxifene, whereas treatment with 10 mg/kg raloxifene yielded full rescue. Notably, left optic nerve axon abundance across all 4 experimental groups was significantly correlated with that eye's contrast sensitivity threshold ($r = 0.248$), suggesting that optic nerve axon loss resulting from the blast injury contributes to the contrast sensitivity deficit and that the rescue of axons with raloxifene treatment contributes to the functional rescue. By contrast, axon abundance was not decreased in right optic nerve of blast-vehicle mice, or in that of raloxifene-treated blast mice, compared to sham. Accordingly, the contrast sensitivity deficit for the right eye, as well as the right eye acuity deficit, must be attributable to something other than optic nerve axon loss.

3.2.2. Melanopsin-expressing ipRGCs

To help elucidate the basis of the changes in light aversion and pupil constriction after blast and with raloxifene treatment, we examined melanopsin-immunolabeled ipRGCs. Given that ipRGC size and melanopsin expression vary with location in the retina, we divided the central two-thirds of the retina into 4 sectors from superior to inferior, as shown in Fig. 1B, and compared only those ipRGCs located in the same sector. As the changes in ipRGC size and melanopsin immunolabeling after blast and with raloxifene treatment were similar across sectors, the data in Fig. 7 are shown relative to the sham values for that sector for each eye. Because there were no consistent differences between the raloxifene doses, we combined the data for the two. For the left eye, ipRGC soma size was significantly decreased and melanopsin immunolabeling was significantly increased for blast-vehicle mice as compared to sham mice. Raloxifene treatment reversed both changes: ipRGC soma size was significantly greater and melanopsin immunolabeling was significantly less for blast-raloxifene mice than for blast-vehicle mice for all sectors. In addition, ipRGC soma size was not significantly less for blast-raloxifene mice than for sham mice for three of the four sectors. The right eye showed similar changes, i.e. a decrease in ipRGC soma size and an increase in melanopsin immunolabeling, which were smaller in extent than for the left eye but still significant for all sectors, and raloxifene rescue of melanopsin expression that reached statistical significance for three of the sectors.

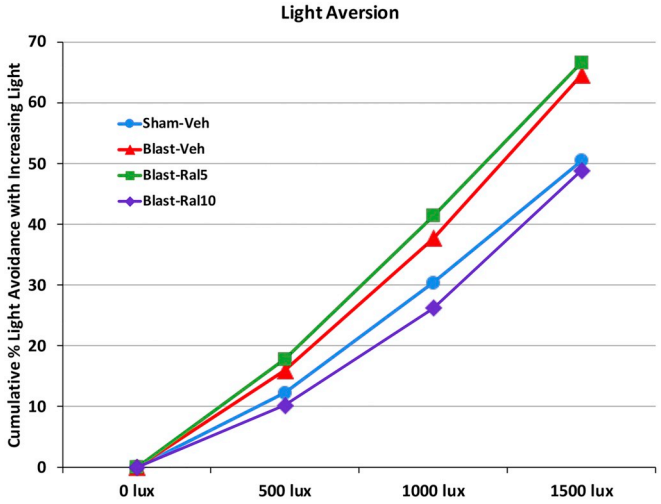

Fig. 4. Light aversion, tested at ~4 months after blast, plotted as cumulative avoidance of an enclosed chamber with increasing brightness, relative to an adjacent dark chamber. Blast-vehicle mice showed greater avoidance of the enclosed chamber as light intensity increased than did sham-vehicle mice (chi-square analysis; $p = .0326$). The amount of enclosed chamber occupancy with increased light intensity for blast-raloxifene10 mice was similar to sham mice ($p = .6242$), but significantly different between blast-raloxifene5 mice and sham ($p = .0029$). Thus, raloxifene at 10 mg/kg, but not at 5 mg/kg, rescued the increase in light aversion.

3.2.3. Oculomotor nucleus

To understand the basis of eye movement abnormalities, we examined the oculomotor nucleus, which innervates 4 of the 6 extraocular muscles, using ChAT immunolabeling. The area occupied by the oculomotor nucleus area was reduced bilaterally by 40.2% and neuron abundance by 32.6% in the blast-vehicle mice compared to sham (Fig. 8). Treatment with 5 mg/kg raloxifene restored OM area and neuron count to levels similar to sham mice and significantly greater than blast-vehicle mice (Fig. 8). Raloxifene at 10 mg/kg also produced significant improvement, but was seemingly somewhat less effective as the lower dose for area. More specifically, OM neuron count for the blast-raloxifene10 mice did not differ significantly from sham mice and was also significantly greater than for blast-vehicle mice, whereas OM area was significantly larger than for blast-vehicle mice but still smaller than for sham mice (Fig. 8).

3.3. Microglial modulation by raloxifene

3.3.1. Effect of raloxifene on optic tract microglia

We examined the right optic tract in tissue sections immunolabeled for IBA1, to visualize all microglia, the M1 marker CD16/32, and the M2 marker CD206, in 5 blast-vehicle mice, 5 blast mice treated with 5 mg/kg raloxifene, and 5 sham mice sacrificed 5 days after blast TBI. We found that blast substantially increased the size of IBA1+ microglia, in accord with our previous findings that microglia in the right optic tract are activated following blast TBI, presumably by molecules released from adjacent damaged axons, and contribute to further axonal

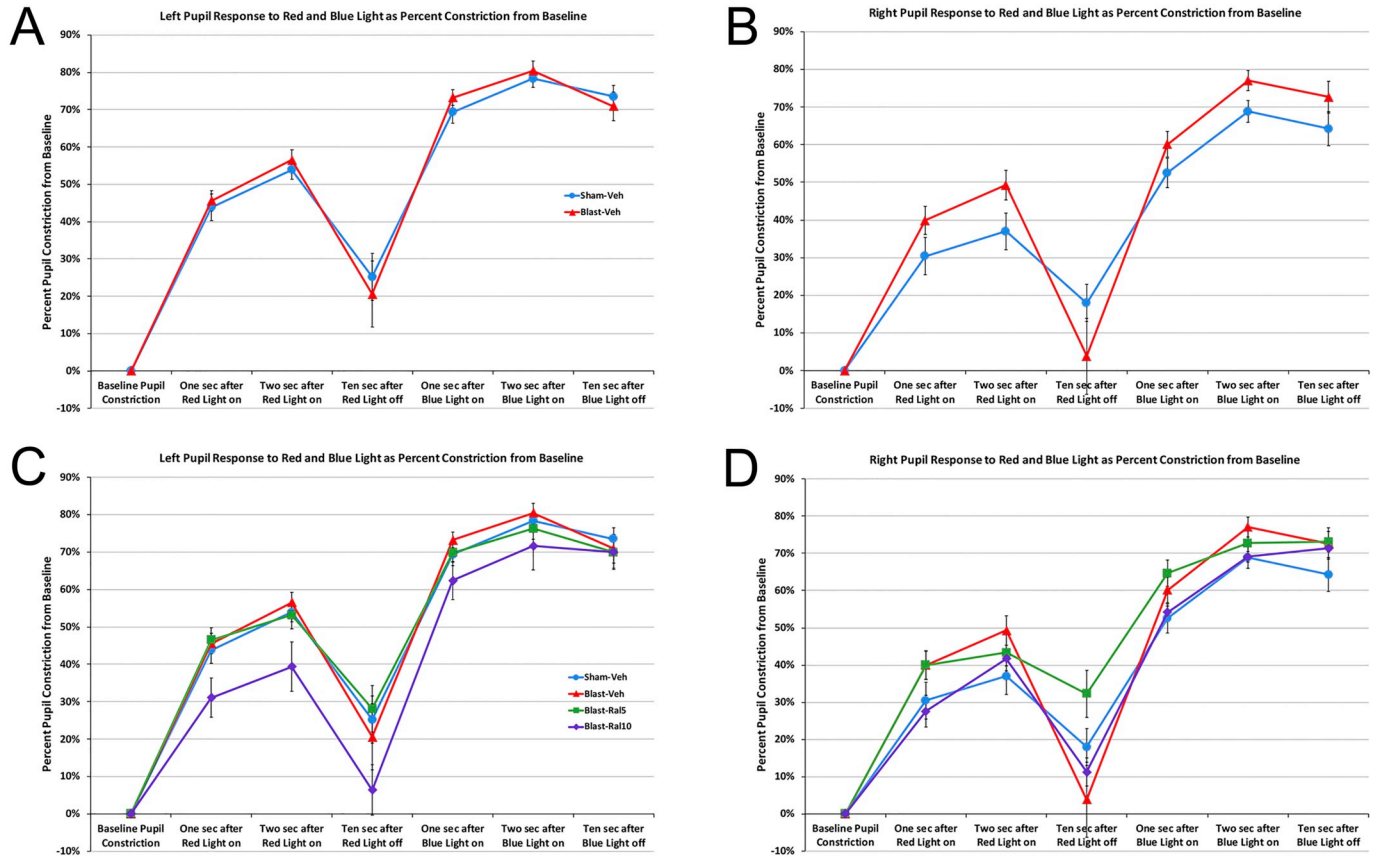

Fig. 5. Pupil responses, plotted as % constriction (i.e. pupil area reduction) from pre-illumination baseline, to red and blue light. **A, C.** Left eye pupil constriction was no different in blast-vehicle mice than in sham mice (A), but blast mice treated with 10 mg/kg raloxifene showed a significantly diminished response to red light ($p = .0012$; C). **B, D.** For the right eye, pupil constriction was significantly enhanced in blast-vehicle mice compared to sham mice during the 2 s of exposure to red light ($p = .0105$), and during and for up to 10 s after exposure to blue light ($p = .005$; B). The pupil responses of mice treated with 10 mg/kg raloxifene were similar to sham for both red light ($p = .836$) and blue light ($p = .363$), whereas pupil constriction for blast-raloxifene5 mice was similar to sham for red light ($p = .0575$), but still enhanced compared to sham for blue light ($p = .0026$; D). Errors bars are SEMs. (For interpretation of the references to colour in this figure legend, the reader is referred to the web version of this article.)

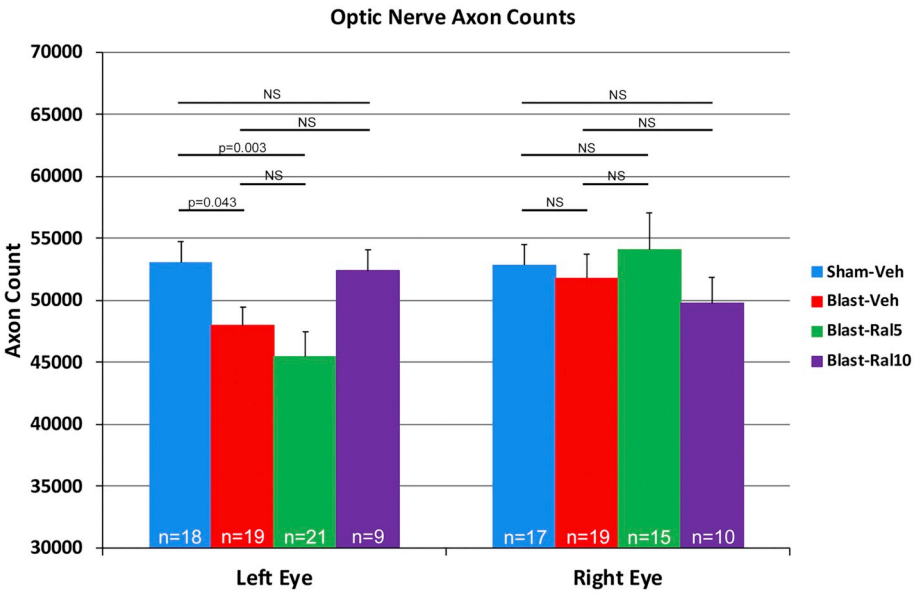

Fig. 6. Optic nerve axon counts. The left optic nerve of blast-vehicle and blast-ral5 mice showed a significant loss of axons. Treatment with 10 mg/kg raloxifene yielded full rescue. The right optic nerve showed no axon loss following blast and none of the differences between experimental groups were significant. N = the number of optic nerves. Errors bars are SEMs.

injury (Guley et al., 2019). Moreover, as shown in Fig. 9, the intensity of IBA1 and CD16/32 immunolabeling was greater in the blast-vehicle mice than in sham-vehicle mice. The intensity of CD206 immunolabeling was also increased, although to a slightly smaller extent than CD16/32 immunolabeling, resulting in a higher M1/M2 ratio for microglia in the blast-vehicle mice than in sham mice (Fig. 9). Quantification of the IBA1 immunolabeling by thresholding and particle analysis also revealed post blast increases in the area occupied by microglia and the density of IBA1+ profiles > 100 pixels in size (~17.4 μm^2). Chi-square analysis showed that microglia in blast-vehicle mice differed highly significantly ($p < 2.0 \times 10^{-107}$) from microglia in sham mice for this combination of six traits. By contrast, the intensity of IBA1 immunolabeling, the areal coverage by microglia and the density of IBA1+ profiles in the right optic tract of blast mice treated with 5 mg/kg raloxifene were all decreased in comparison to blast-vehicle mice (Fig. 9). Further, CD16/32 expression was decreased relative to blast-vehicle mice, while CD206 expression was increased, reducing the M1/M2 ratio to a level similar to that for the sham mice. Chi-square analysis for the six traits showed a significant difference ($p = .0051$) between microglia in the blast-raloxifene mice and the blast-vehicle mice. Thus, raloxifene treatment appears to partially reverse microglial activation, and bias microglia toward the protective M2 state.

3.3.2. qPCR studies of microglia modulation over time after blast TBI

To expand our understanding of microglial modulation after blast beyond our current and previous findings using immunofluorescent labeling (Bu et al., 2016; Guley et al., 2016, 2019), we used qPCR to quantify the expression of 4 M0 markers, 5 M1 markers, and 4 M2 markers in left and right optic nerve, retina, and thalamus at 1, 3, and 5 days after blast (Fig. 10A-F). The M1 markers tended to show the greatest changes over this 5-day time period, with multiple M1 markers being elevated for each tissue at least at one time point. In particular, each of the 5 M1 markers was increased > 50% in left optic nerve (LON), left retina, and both left and right thalamus at 3 days, and 3 of the 5 markers (TNFα, IFNγ and IL1β) were increased > 50% in right optic nerve (RON) and right retina at 5 days (Tables 2–4 in the supplementary material). The expression of the 5 M1 markers averaged together exhibited a larger peak increase during the 5-day period after blast than did the expression of the M2 (and M0) markers for both sides of the retina and the thalamus. By contrast, the M2 markers showed a larger peak increase than the M1 (and M0) markers for left and right optic nerves. In fact, the M0 markers changed fairly little after blast (< 50%), the only exception being the left retina.

The increase in M1 marker expression was transient over the 5-day time period we examined. M1 transcript levels in LON and left and right thalamus increased from day 1 to day 3, and declined by day 5. The left retina also showed an M1 decline at day 5, although its M1 expression was already high at day 1, and remained high at day 3. In contrast, M1 expression in right retina was low at day 1, slightly elevated at day 3, and considerably increased by day 5, and RON showed only small changes in M1 expression but followed a similar temporal pattern, with M1 levels higher at day 5 than at day 3. Changes in M2 expression also appeared to be transient in the case of RON and right thalamus, for which the expression of the 4 M2 markers averaged together increased from day 1 to day 3 but declined by day 5. In contrast, for LON, left and right retina, and left thalamus, M2 expression was low at day 3 but increased by day 5. Whether this increase in M2 expression persisted beyond day 5, or whether M2 levels showed a rapid decline similar to M2 expression for RON and right thalamus between days 3 and 5 is uncertain.

To help visualize the temporal changes in relative M1 versus M2 expression levels, we calculated M1/M2 ratios for each time point for each tissue. Left optic nerve, retina and thalamus exhibited an M1/M2 peak at 3 days followed by decline at 5 days, whereas M1/M2 ratios were higher at 5 days than at 3 days for these same tissues on the right side (Fig. 10G). Thus, the natural progression in microglial behavior appears to entail M1 activation during the first 3 days after injury, with a gradual overtaking of M1 markers by M2 markers by 5 days for the directly targeted left side and a delayed increase in M1 expression relative to M2 expression on the contrecoup right side, indicating different pathogenic processes on the right than on the left.

3.3.3. qPCR studies of raloxifene effects on microglial modulation after blast TBI

To examine how raloxifene affects microglia, mice were treated 2 h after blast, again on days 1–3, sacrificed, and qPCR performed as described above. As shown in Fig. 11A-F, raloxifene treatment generally decreased the expression of M1 markers and increased the expression of M2 markers over their respective levels in blast-vehicle mice, with the higher dose generally being more effective. More specifically, 10 mg/kg raloxifene decreased M1 expression and increased M2 expression for the retina and the thalamus on both sides, whereas 5 mg/kg raloxifene increased M2 markers but did not decrease M1 markers in the retina, and decreased M1 markers but did not notably increase M2 markers in the thalamus. In the case of the left optic nerve, the higher dose of raloxifene decreased M1 expression but did not increase M2 expression,

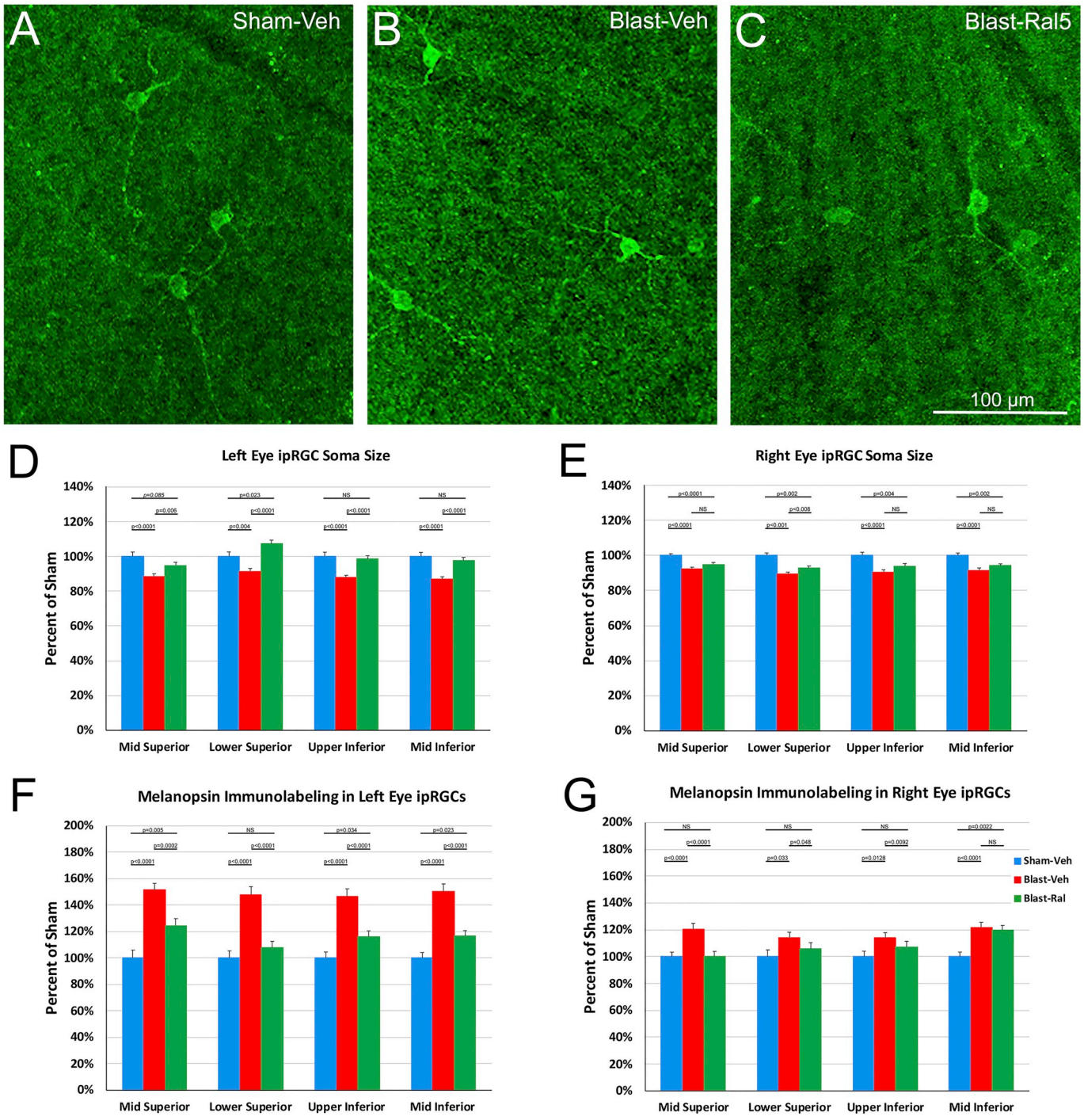

Fig. 7. Melanopsin + ipRGC analysis. **A-C.** Confocal images of melanopsin immunolabeling, all taken from the mid-inferior sector of the left eye. ipRGC cell bodies in the blast-vehicle retina were more intensely immunolabeled for melanopsin and smaller than in the sham. These changes were largely reversed in raloxifene-treated mice. Scale bar in C applies to A-C. **D-G.** Quantification of soma size and melanopsin immunolabeling, shown relative to the sham value for each sector for each eye. Blast significantly reduced ipRGC size and increased melanopsin immunolabeling for both eyes. Raloxifene treatment consistently lessened the effect of blast. Errors bars are SEMs. *p* values that are close to statistical significance are shown italicized.

while the lower dose increased M2 expression but did not decrease M1 expression. For the right optic nerve, both doses increased M2 expression, the higher dose to a greater extent, but both had little effect on M1 expression (Fig. 11G). M1/M2 ratios for the blast-vehicle mice were > 1 for all tissues, with the exception of RON, consistent with the early modulation of microglia toward the M1 state following injury. M1/M2 ratios for the raloxifene-treated mice were lower than for the blast-vehicle mice for all 6 tissues for both doses, consistent with raloxifene modulating microglia toward the M2 state. Moreover, the M1/M2 ratios were lower for the 10 mg/kg dose than the 5 mg/kg dose for all but LON, suggesting the higher dose is generally more effective than the lower dose in modulating microglia. With respect to specific transcripts, the two doses of raloxifene exhibited some similarities and some differences (Tables 5–7 in the supplementary material). For example, both doses increased all M2 markers in left retina (note IL10 levels were too low to detect in the raloxifene10 retinal samples), and all but TREM2 in RON. However, while the lower dose increased all M2 markers in LON and left thalamus, the higher dose increased only 3 of

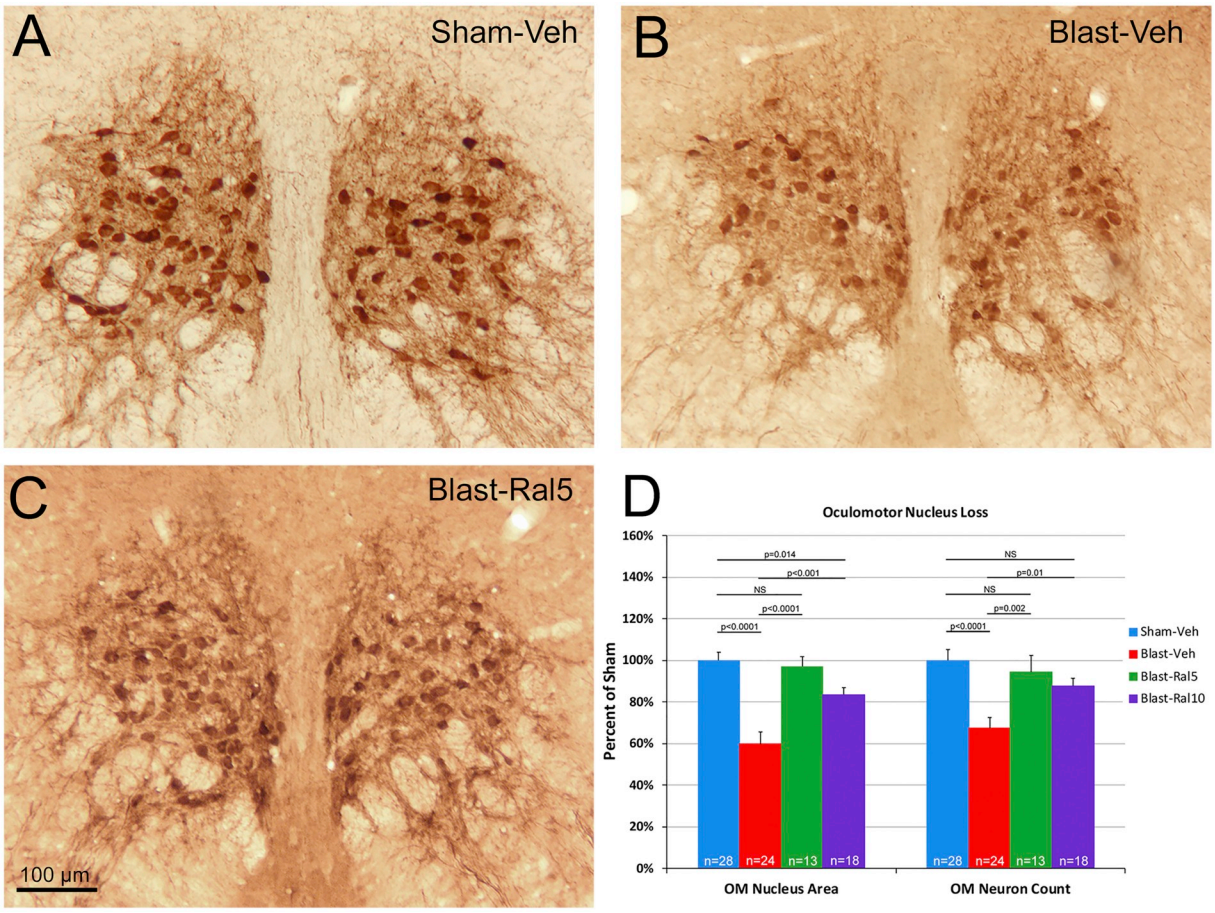

Fig. 8. Oculomotor nuclei. **A-C.** Sections of midbrain immunostained for choline acetyltransferase to reveal motoneurons. The area occupied by the oculomotor (OM) nucleus and its neuron abundance were less on both sides of the blast-vehicle mouse than in the sham, whereas mice treated with 5 mg/kg raloxifene were similar to sham. Scale bar in C applies to A-C. **D**. Quantification of OM nucleus area and number of neurons. The left and right sides for each mouse were pooled for statistical analysis. Raloxifene treatment yielded rescue, with 5 mg/kg being somewhat more effective than 10 mg/kg for both parameters. N = number of OM nuclei analyzed. Errors bars are SEMs.

the 4 M2 markers in these same tissues (all but YM1 in LON and all but TREM2 in left thalamus).

3.4. CB2 inverse agonist specificity of raloxifene benefit

3.4.1. CB2 receptor pharmacology

We previously demonstrated the inverse agonism of SMM-189 at CB2 receptors by assessing its ability to increase cAMP in cells expressing CB2 receptors (Presley et al., 2015). To confirm raloxifene action as an inverse agonist at CB2 receptors (Kumar and Song, 2013), we used the ACTOne cell-based cAMP assay in HEK-CNG + CB2 cells. Raloxifene caused a dose-dependent increase in cAMP-driven fluorescence with 1 μM of drug producing a level of fluorescence over baseline 5-fold greater than that for SMM-189 (Fig. 12). Thus, raloxifene appears to provide greater efficacy as a CB2 inverse agonist than SMM-189.

3.4.2. Raloxifene benefit is mimicked by the CB2 inverse agonist SR144528

We next evaluated if the selective CB2 inverse agonist SR144528, which we have previously shown increases the levels of M2 markers on the surfaces of cultured microglia (Presley et al., 2015), similarly yields rescue for the contrast sensitivity deficit after blast. As shown in Fig. 13A, SR144528 rescued the TBI-induced contrast sensitivity deficit for both eyes.

3.4.3. Raloxifene benefit does not depend on its estrogenic effects

In principle, raloxifene benefit could stem, not from its action on CB2 receptors, but rather via its agonist effects on β-type estrogen receptors, or its antagonism at α-type estrogen receptors (Frick et al., 2015; Habib and Beyer, 2015). To test the first possibility, we treated some blast mice with 5 mg/kg raloxifene immediately followed by the ER-β antagonist PHTPP. To test both possibilities, we injected other mice successively with a selective ER-β agonist (DPN) and a selective ER-α antagonist (MPP). An additional set of mice received 5 mg/kg raloxifene and then a saline injection. Drug administration followed our typical two-week schedule. Subsequent contrast sensitivity testing showed that, as expected, raloxifene followed by saline rescued the deficit for both eyes (Fig. 13B). The ER-β antagonist PHTPP did not attenuate the rescuing effect of raloxifene for either eye, and the combination of DPN and MPP did not replicate raloxifene rescue. Our findings that blocking the ER-β agonism of raloxifene does not prevent benefit, and mimicking the ER-β agonism and selective ER-α antagonism of raloxifene does not replicate raloxifene benefit, indicate that the estrogenic actions of raloxifene are not the basis of its ability to mitigate visual deficits after blast TBI.

3.5. Raloxifene treatment window for functional benefit after blast TBI

To determine if delaying administration of raloxifene still yields benefit, we used 5 mg/kg as the standard dose and varied the treatment regimen as follows. One group of mice first received raloxifene one day after blast (thus missing treatment on day 0, the day of blast), and was then treated daily for 14 days (blast-ral day 1–14). A second group of

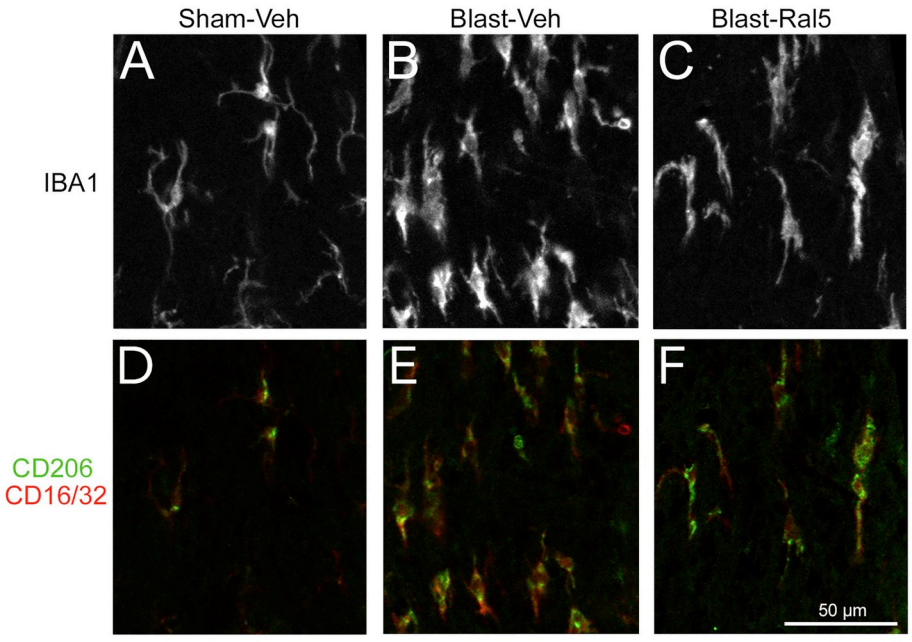

G

	IBA1 OD	CD16/32 OD	CD206 OD	M1/M2	# IBA1+ profiles/mm^2	% IBA1 areal coverage
sham	12.5	10.5	11.2	0.96	598	4.7%
blast-vehicle	17.7	12.6	12.7	1.00	990	14.4%
blast-ral5	16.9	12.3	13.0	0.94	807	11.6%

Fig. 9. Microglia in right optic tract. A-E. Confocal images showing the right optic tract of a Sham-Veh mouse (A, C), Blast-Veh (B, E), and a Blast-Ral5 mouse (D, F), simultaneously immunolabeled for Iba-1 to visualize microglia, for CD16/32 to detect the M1 phenotype, and for CD206 to detect the M2 phenotype. The upper panels show the IBA1 immunolabeling pseudo-colored white, while the lower panels are of the same field of view as the panel immediately above and show the merge for the M1 and M2 markers. The red CD16/32 M1 labeling predominates more in the Blast-Veh image in E than in the corresponding Blast-SMM image in F, where the green CD206 M2 labeling is more readily seen. The scale bar in F applies to A-F. G. Quantification of the IBA1, CD16/32 and CD206 immmunolabeling. The intensity of IBA1, CD16/32 and CD206 immunolabeling, the M1/M2 ratio, microglial abundance and areal coverage are all increased by blast, as also shown in B and E compared to A and D, respectively. Raloxifene treatment decreased microglial abundance and areal coverage, and the intensity of IBA1 and CD16/32 immunolabeling compared to Blast-Veh, but increased CD206 immunolabeling intensity and thus decreased the M1/M2 ratio, as seen in images C and F compared to B and E, respectively. (For interpretation of the references to colour in this figure legend, the reader is referred to the web version of this article.)

mice was not treated until the second day after blast (blast-ral day 2–14) and a third group not until the third day (blast-ral day 3–14). For comparison, a fourth group of mice received only 4 daily treatments (blast-ral day 0–3). As shown in Fig. 14, the left eye contrast sensitivity threshold for mice first treated the day after blast, or two days after blast did not differ significantly from sham mice. However, the left eye contrast sensitivity threshold for mice first treated on the third day of blast differed significantly from sham mice, as did that for mice treated for only the first 3 days. Thus, a delay in raloxifene treatment until the second day after blast still yielded rescue of the blast-induced contrast sensitivity deficit for the left eye, whereas a longer delay or a shorter treatment failed to provide benefit. By contrast, the contrast sensitivity and visual acuity deficits for the right eye were both rescued by all 4 treatment regimens, indicating a wider treatment window pertains for some TBI outcomes.

4. Discussion

In the work described here, we report that raloxifene rescues a variety of visual deficits and associated pathologies that would otherwise result from TBI. Below we describe these deficits and pathologies, the relationships between them, and their rescue by raloxifene. We then move on to discuss the mechanism of raloxifene action and its potential as a therapy for patients suffering from TBI.

4.1. Visual deficits and pathology associated with blast

As previously described for our left-side focal cranial blast TBI model (Guley et al., 2016), as the blast pressure wave crosses the skull and passes from left to right, the brain is likely to move rightwards in the cranium and then recoil. The associated stretch, stress, and shear forces injure axons, as is evidenced by the presence of swollen axonal bulbs a few days after the injury. The damaged axons are conspicuously associated with microglia that have been activated by molecules released from the axons and their ensheathing myelin. These microglia are primarily biased toward the pro-inflammatory M1 state, exacerbating the injury (Loane and Kumar, 2016; Donat et al., 2017) and serving as the target of our raloxifene treatment strategy. We have found damaged RGC axons, surrounded by activated microglia, primarily at three sites in our focal cranial blast model: as they exit the left eye to enter the optic nerve, as they traverse the narrow bony optic nerve canal, and as they project along the right optic tract (Guley et al., 2019). Some of the initial axonal injury reflects damage severe enough to progress to degeneration, as ~10% of axons in the left optic nerve are lost by 30 days after blast (here and Guley et al., 2019). The RGC axon loss appears to contribute to the contrast sensitivity deficit for the left eye, based on the significant correlation between these two parameters (here and Guley et al., 2019). In addition, raloxifene treatment rescued both the optic nerve loss and the contrast sensitivity deficit, suggesting that the functional rescue, at least in part, stems from the rescue of optic nerve axons. A similar relationship does not pertain to the right eye, which shows a contrast sensitivity deficit, but little, if any, loss of optic nerve axons (here and Guley et al., 2019). The right eye contrast sensitivity deficit may instead be caused by retinal injury (discussed below), optic nerve dysfunction not manifesting as loss, and/or injury to central visual areas on the left (blast) side of the brain to which the right eye projects. Raloxifene rescue would then result from the amelioration of the relevant perturbation.

The biomechanical forces resulting from the blast pressure wave could potentially cause injury to, not just the optic nerve, but other cranial nerves as well. Of importance for visual function, these include the oculomotor, trochlear, and abducens nerves, which together innervate the six extraocular muscles. Consistent with this possibility, we found a > 30% loss of motoneurons in the oculomotor nucleus (which innervates 4 of the 6 extraocular muscles). That the extent of this neuron loss was the same for the two sides of the brain and considerably greater than the 10% loss of left optic nerve axons raises the additional possibility that oculomotor cell bodies, despite their location some distance from the blast, were directly damaged. Indeed we have previously found bilateral neuron loss in the cortex and striatum (20% and

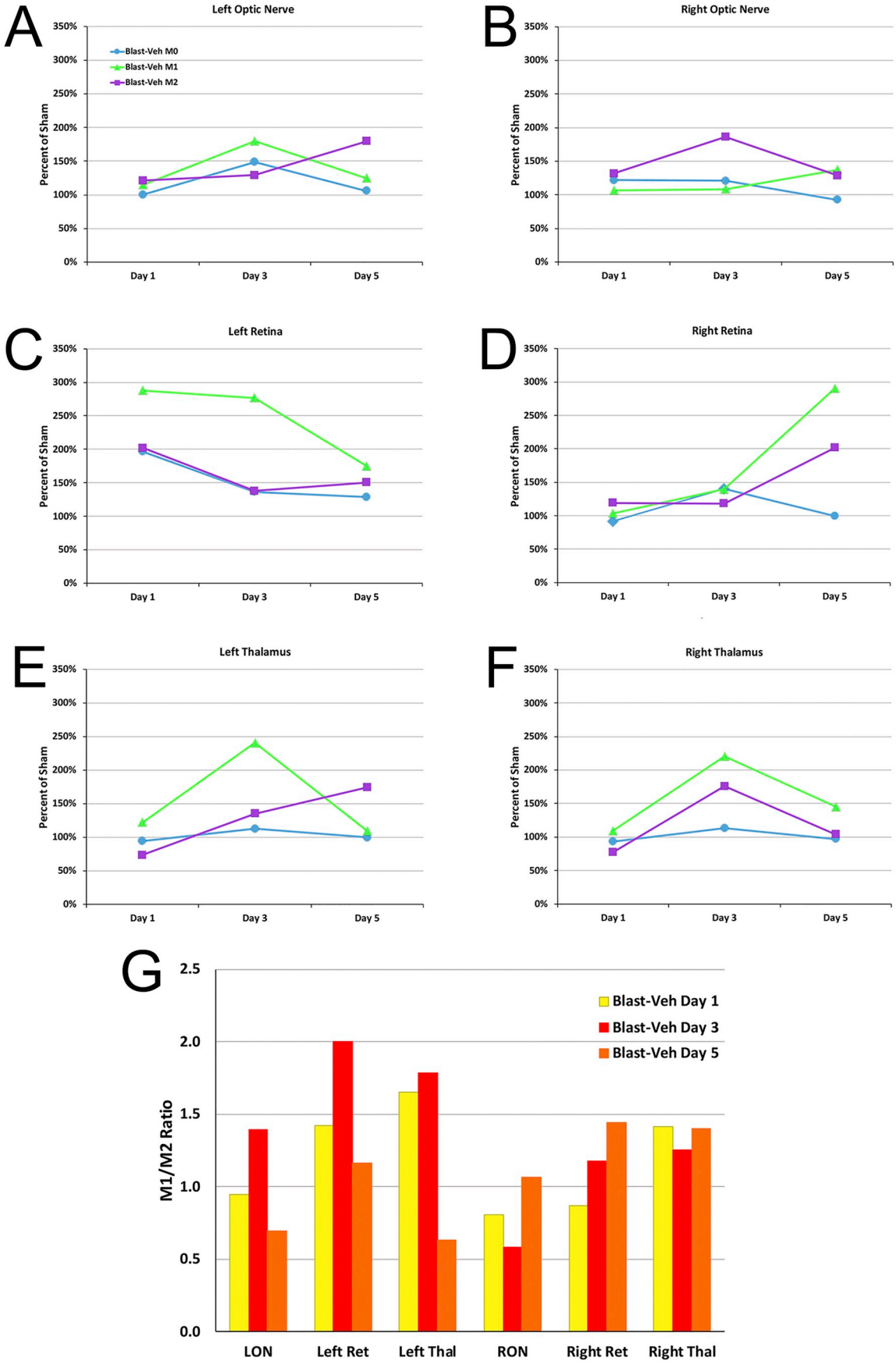

(caption on next page)

Fig. 10. The mean expression of M0, M1, and M2 markers with time after blast. **A-F.** Transcript levels were determined by qPCR and are expressed relative to transcript levels for the same tissue from sham-vehicle mice. The blast-induced changes in transcript levels were the largest for M1 markers, and the smallest for M0 markers. Additionally, M1 marker increases were greater on the left side than on the right side for corresponding tissues at 3 days, but greater on the right at 5 days. **G.** Transcript levels are expressed as M1/M2 ratios to help visualize temporal changes in expression. For the left side, the M1/M2 ratio peaks at 3 days. By contrast, for right side the M1/M2 ratio is higher at 5 days than at 1 or 3 days (optic nerve and retina), or fairly similar at all time points (thalamus).

30%, respectively; Bu et al., 2016), even among cortical neurons with axons projecting locally rather than along a white matter tract. Regardless of the mechanism(s) of injury, the loss of oculomotor innervation would lead to impaired control of the extraocular muscles and thereby probably contribute to the deficits in fixation, pursuit, saccades, and vergence frequently exhibited by human victims of TBI (Goodrich et al., 2013; Capó-Aponte et al., 2017). Importantly, we found that raloxifene treatment prevented the loss of oculomotor neurons, as we have previously shown for SMM-189 in the case of cortical and striatal neurons (Bu et al., 2016), suggesting that microglial activation somehow contributes to neuron loss. Treatment with raloxifene might thereby reduce eye movement dysfunction and the various visual deficits mentioned above in human TBI victims.

Despite the eyes being shielded from the blast, we also observed retinal injury in the form of reductions in peak amplitude of the photoreceptor-driven A-wave for both eyes and in the bipolar-cell driven B-wave for the left eye. The reduction of both ERG components for the left retina is consistent with our previous observations of increased microglial abundance at 3 and 30 days (Guley et al., 2019), upregulation of glial fibrillary acidic protein (GFAP) at 30 days (Guley et al., 2019), and thinning, of inner retina in particular, by 11 weeks in the left eye following left side focal cranial blast (Reiner et al., 2015). The damage to the left eye may originate from the torsion/stretch of soft tissues accompanying the transmission of blast wave through the orbit, and may in turn factor into the impairment of contrast sensitivity. For the right retina, we previously reported two signs of injury: an increase in microglial abundance at 30 days (Guley et al., 2019) and thickening of the inner retina at 11 weeks (Reiner et al., 2015). Pathology for the right eye appears to be delayed and/or progress more slowly than for the left eye (Reiner et al., 2015; Guley et al., 2019) and the underlying mechanism(s) is/are uncertain. One possibility is that the right eye is subjected to compressive forces as the head is pushed toward the right during left side blast (Bricker-Anthony and Rex, 2015). We have not detected retinal detachment or obvious damage to the cornea, as reported after a direct ocular blast at 26-psi (Hines-Beard et al., 2012; Bricker-Anthony et al., 2014, 2017) but not at 15-psi blast (Vest et al., 2019), perhaps because the right side of the mouse head is cushioned by soft foam in our experimental setup. Nonetheless, the thickening of inner retina we have observed, possibly reflecting an underlying edema, may contribute to the right eye contrast sensitivity and visual acuity deficits. Importantly, raloxifene rescued the ERG deficits for both eyes, despite the differing retinal pathologies, suggesting that microglial responses contribute to pathogenesis in the retina and poor visual function in both eyes following TBI.

The mice subjected to blast also exhibited increased light aversion and enhanced pupil constriction of the right eye. To help understand the basis of these functional impairments, we focused our retinal analysis on melanopsin-expressing ipRGCs, which constitute 2–3% of the total population of RGCs (Hughes et al., 2013). IpRGCs have been implicated in light aversion (Collison et al., 2015; Matynia et al., 2012) and, through their projections to the olivary pretectal nucleus (Baver et al., 2008), mediate pupillary responses to blue light (Schmidt et al., 2011). Moreover, the downregulation of melanopsin levels by ipRGCs is associated with diminished pupil light responses (Ouk et al., 2016). Here we found ipRGCs in both eyes increased their levels of melanopsin and became smaller in size after blast, with changes for left retina greater than for right retina. Raloxifene rescued the increased light aversion and the enhanced right eye pupil constriction, as well as the upregulation of melanopsin levels and the decrease in ipRGC cell size for both eyes. One possible scenario is that the increased melanopsin expression contributes to the greater light aversion and to the enhanced pupil constriction for the right eye after blast, while the potential for hyper-pupil responsiveness is counteracted by optic nerve axon loss for the left eye. Alternatively, or in addition, the increased light aversion after blast may stem from a putative similar upregulation of melanopsin expression by the recently identified subpopulation of nociceptive trigeminal neurons localized primarily to the ophthalmic branch of the trigeminal nerve (Matynia et al., 2016), which innervate cornea. Additional trigeminal afferent fibers supplying the conjunctiva, cornea, sclera, and/or uvea may also transmit pain signals that contribute to photophobia (Matynia et al., 2015).

4.2. Microglial modulation by TBI and raloxifene

As described above, microglia in the retina, optic nerve and brain become activated after blast TBI, and confirmed here for the right optic tract. While some investigators have reported benefit using CB2 agonists (Magid et al., 2019), CB2 inverse agonists have the advantage of stabilizing CB2 receptors in an inactive state, which leads to transcriptional changes whereby microglia are biased away from the pro-inflammatory M1 state and toward the protective M2 state (Lunn et al., 2006, 2008; Lawrence and Natoli, 2011; Franco and Fernández-Suárez, 2015). We previously showed that the CB2 inverse agonist SMM-189 has this effect on microglia in vitro using biochemical approaches (Presley et al., 2015; Reiner et al., 2015) and in vivo using immunostaining (Bu et al., 2016; Guley et al., 2019). Importantly, SMM-189 treatment rescued various sensory, motor and emotional deficits that mice otherwise exhibit after TBI and the accompanying axon and neuron loss (Reiner et al., 2015; Bu et al., 2016; Guley et al., 2019). SMM-189, however, has not undergone any human testing, and so the possibility that it could be used as a human TBI therapy is at least a decade off. Similarly, the commercially available CB2 inverse agonist SR144528, although effective in vitro (Presley et al., 2015) and in rescuing deficits in contrast sensitivity (Fig. 13 in the current studies), is not approved for human use. Such impediments do not apply to raloxifene, which is already FDA-approved as a selective estrogen receptor modulator, but also possesses CB2 inverse agonism, as first shown by Kumar and Song (2013) and confirmed here using the ACTOne assay.

Although we describe microglia here as having two distinct polarization states, we well realize that this is an oversimplification. Rather, microglia appear to be remarkably diverse, comprising a multidimensional spectrum of phenotypes when numerous characteristics of individual cells are profiled (Hanisch, 2013; Franco and Fernández-Suárez, 2015; Jha et al., 2016; Morganti et al., 2016; Fernández-Arjona et al., 2017). In the current work, we used qPCR to characterize microglia, so that we could simultaneously assess expression of a greater number of markers than in our previous and current studies using immunostaining (Bu et al., 2016; Guley et al., 2019). While our approach has the disadvantages that we could not examine microglia for this number of markers on an individual basis and that changes in transcript levels (of TGFβ, for example) might in some cases reflect not just microglia, but other cell types as well (Doyle et al., 2010; Dobolyi et al., 2012), it provides a more comprehensive view of the overall inflammatory/protective milieu. Note, however, that seven of the 13 transcripts we examined are unique to microglia (IBA1, Tmem119, P2ry12, CD16/32, IL1β, Ym1, and TREM2). Further, the immunolabeling results we present here indicate that blast and raloxifene

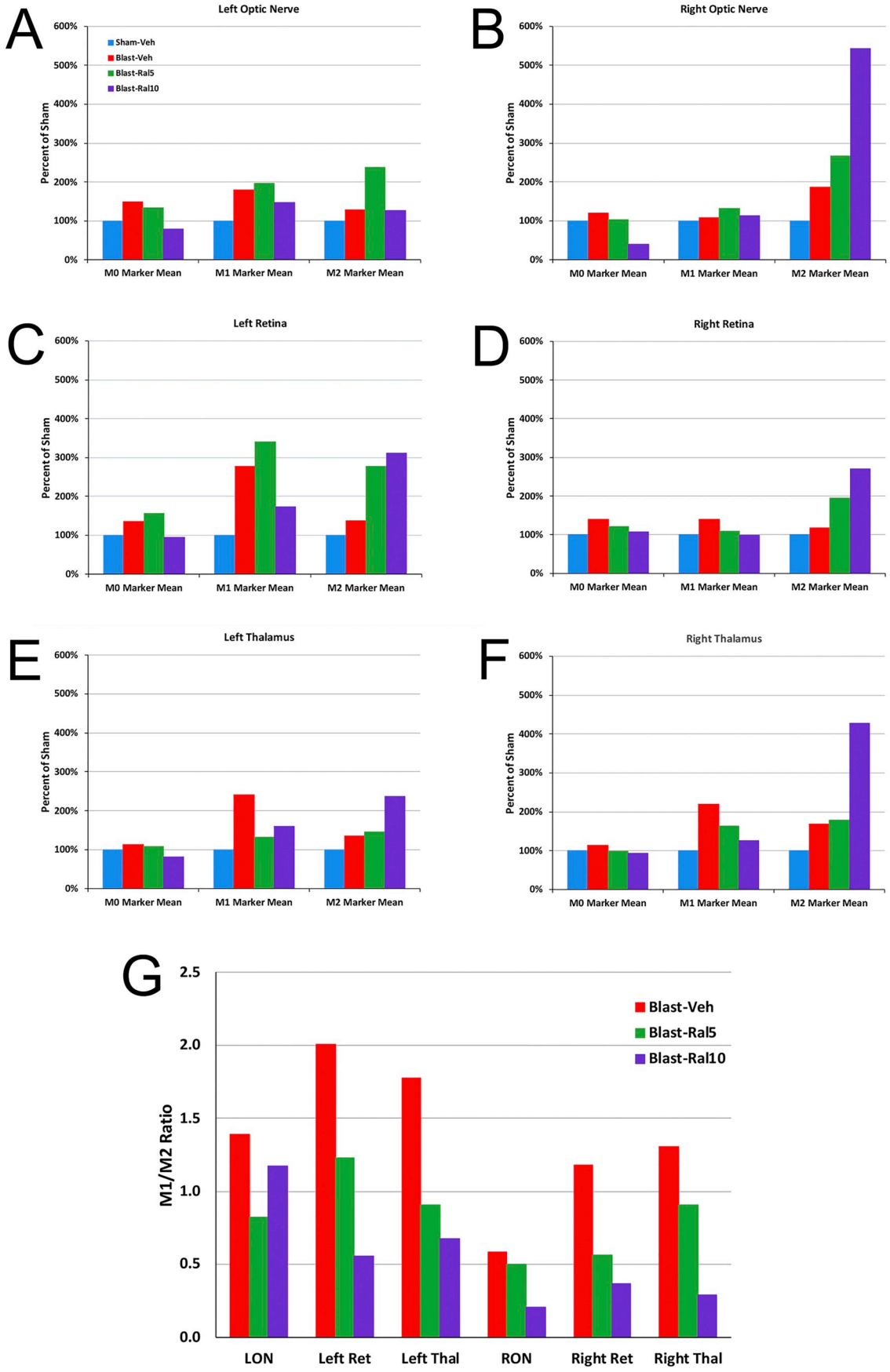

(caption on next page)

Fig. 11. The mean expression of M0, M1, and M2 markers at 3 days after blast. **A-F.** Transcript levels were determined by qPCR and are expressed relative to transcript levels for the same tissue from sham-vehicle mice. Expression of M1 markers relative to M2 markers was increased following blast for all tissues except RON. M1 expression levels were decreased by raloxifene at the higher dose, and in some cases at the lower dose. Raloxifene also increased M2 expression in 4 of the 6 tissues, with the higher dose being more effective than the lower dose, except for LON. **G.** Raloxifene reduced the M1/M2 ratio below blast-vehicle for optic nerve, retina and thalamus on both sides, with the higher dose being more effective than the lower dose, with left optic nerve being the only exception.

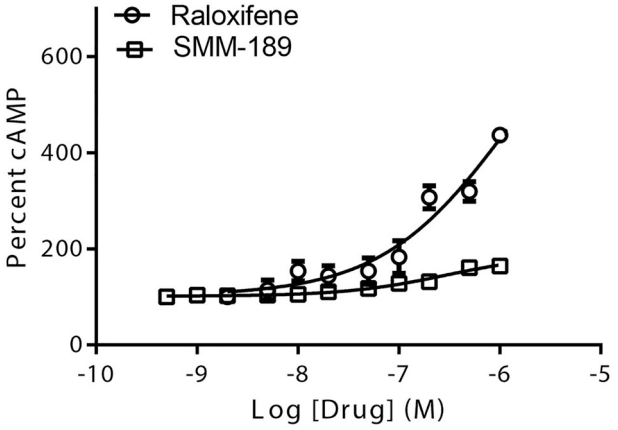

Fig. 12. Comparison of raloxifene and SMM-189 activity in HEK-CNG + CB2 cells using the ACTOne assay. Raloxifene caused a dose-dependent increase in cAMP-driven fluorescence over baseline that was about 5-fold greater than that with SMM-189 at a concentration of 1 μM.

exert effects on microglia in the right optic tract and are in concordance with the qPCR results for the markers examined in common (IBA1 and CD16/32). In our qPCR studies, we found considerable variation between the different tissues and the sides of the animal (coup-contrecoup) in the time course of changes in microglial markers, yet several patterns were evident. M0 markers changed little after blast, rarely by > 50%, while M1 markers often increased 2–3-fold. M2 marker expression tended to be low initially after blast, especially compared to M1 markers, and later increased. This pattern was most evident for the left optic nerve, retina, and thalamus, for which the M1/M2 ratio peaked at 3 days and declined below the 1-day level by 5 days (Fig. 10G). Thus, the natural progression in microglial behavior for the directly targeted left side appeared to entail M1 activation during the first 3 days after injury, with a gradual decline of M1 markers and an increase in M2 markers by 5 days. Interestingly, a similar pattern of initial M1 activation followed by M2 activation has been reported following controlled cortical or closed head impact TBI (Morganti et al., 2016; Kumar et al., 2016; Madathil et al., 2018), which produce greater injury than our air blast model. By contrast, M1 expression and the M1/M2 ratio for RON and right retina did not increase until or continued to increase at day 5, indicating a different and slower pathogenic mechanism for the contrecoup side, either because the level of pressure reaching the right side is less or because the tissue distortion caused by left side blast differs for the two sides. Temporal changes in microglial expression for the right thalamus differed from that of the other 5 tissues in that its M1/M2 ratio was high for all 5 days after blast, perhaps because the right thalamus contains the brain continuation of the directly damaged left optic nerve (i.e. the right optic tract) and its central targets, and thus exhibits both coup and contrecoup characteristics.

Our qPCR results further showed that the expression of microglial markers at 3 days after blast was modulated by raloxifene treatment. Both doses of raloxifene reduced the M1/M2 ratio for all tissues below that for blast-vehicle mice and one or both doses reduced the M1 expression below blast-vehicle levels in 5 of the 6 tissues, the higher dose generally being more effective. For example, 10 mg/kg raloxifene decreased M1 expression and increased M2 expression for both sides of retina and thalamus, whereas 5 mg/kg raloxifene effects were limited to increasing M2 markers in the retina, and to decreasing M1 markers in the thalamus. The results for raloxifene effects on the left optic nerve were different than for all the other tissues in that not even the higher dose both decreased M1 expression and increased M2 expression, but it nonetheless rescued the loss of left optic nerve axons. It is possible that treatment with the higher dose for more than the 4 days used in the case of the qPCR studies would be effective in decreasing M1 markers and increasing M2 markers, as treatment continued for 15 days in the case of all the histological assessments and functional testing. Indeed, only the higher dose was able to rescue the increase in light aversion, and microglial activation clearly persists for longer than a few days after blast injury. It should, however, also be noted that for some outcomes, for example right eye visual acuity, the lower dose possibly provided better rescue than the higher dose. The reasons for the variation in the amount of rescue for the two doses we tested are not clear, although they do not appear to reflect any drug toxicity, as the raloxifene-treated

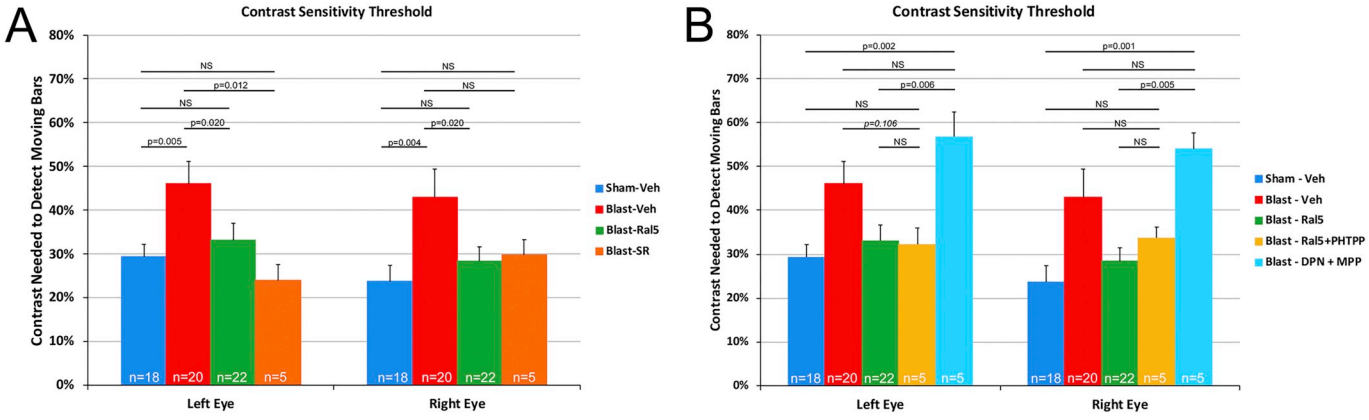

Fig. 13. Comparison of raloxifene with other drugs on the rescue of contrast sensitivity deficits produced by blast TBI. **A.** Comparison of raloxifene and the CB2 inverse agonist SR144528. The SR144528 benefit was similar to that observed with raloxifene. **B.** Comparison of raloxifene with drugs acting at estrogen receptors. Injection of the ER-β antagonist PHTPP immediately following injection of 5 mg/kg raloxifene did not lessen the benefit of raloxifene. Injection of the ER-β agonist DPN followed by the selective ER-α antagonist PHTPP yielded no benefit, rather than duplicating raloxifene action. Statistical comparisons between sham-vehicle, blast-vehicle, and blast-ral5 are the same as in panel A, but for simplicity, are not shown in panel B. N = the number of eyes. Errors bars are SEMs. p values that are close to statistical significance are shown italicized.

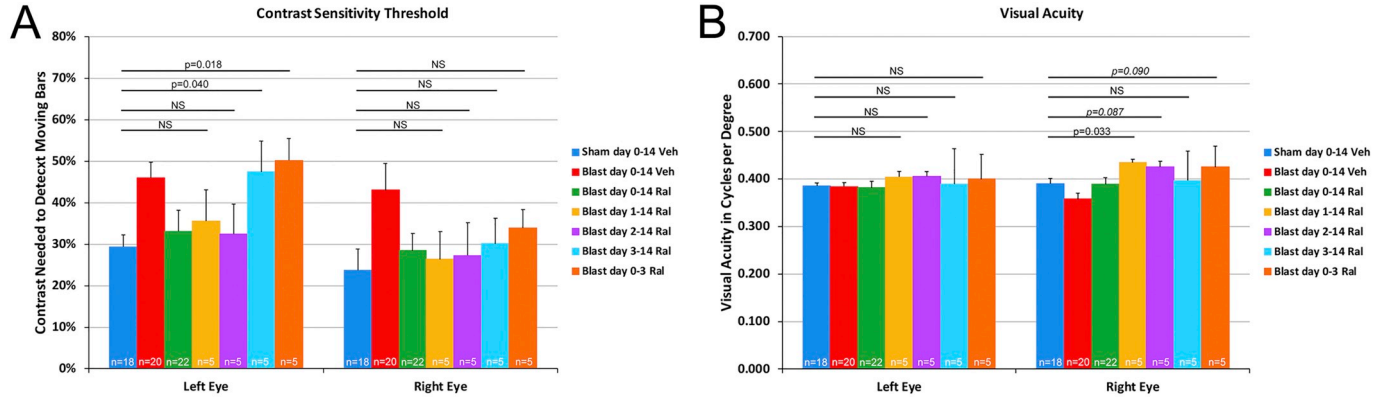

Fig. 14. Effective treatment windows for raloxifene rescue of deficits in contrast sensitivity and acuity. Raloxifene treatment was delayed for 1, 2 or 3 days in separate groups of mice or discontinued starting four days after blast. **A.** The contrast sensitivity deficit for the left eye was rescued even when raloxifene treatment was delayed for 2 days after blast, but not when treatment was either delayed for 3 days or did not continue past the third day. By contrast, the contrast sensitivity deficit for the right eye was rescued regardless of treatment regimen. **B.** The visual acuity deficit for the right eye was rescued by all 4 of the treatment schedules. There was no visual acuity deficit for the left eye. N = the number of eyes. Errors bars are SEMs. p values that are close to statistical significance are shown italicized.

mice (at either dose) did not weigh less than sham or blast-vehicle mice at the time of sacrifice. Moreover, mice have been shown to survive doses as high as 5000 mg/kg without obvious untoward effects (Raloxifene FDA Drug Approval Package, 1999). Nonetheless, optimization of raloxifene dosage will require further attention and would certainly be a component of any future human trials, as discussed in the following section.

4.3. Considerations for human use

In principle, raloxifene benefit could stem, not from its action on CB2 receptors, but rather from its estrogenic effects. This does not seem to be the case, since we found that the ER-β antagonist PHTPP did not block, and the ER-β agonist DPN in combination with the selective ER-α antagonist did not duplicate the raloxifene rescue of the contrast sensitivity deficit after blast TBI. Thus, the benefit we observed with raloxifene in mitigating visual system dysfunction and injury appears to derive from its CB2 actions rather than its estrogenic effects. Moreover, another CB2 inverse agonist, SR144528, duplicated the benefit of SMM-189 and raloxifene for the contrast sensitivity deficit after TBI in our blast model.

Raloxifene was first approved by the FDA to treat postmenopausal osteoporosis nearly twenty years ago and has since been approved to reduce the risk of invasive breast cancer in postmenopausal women. Importantly, raloxifene has no evident adverse hormonal side effects and is safe for use in men, having been tested in clinical trials to treat bone fracture (Uebelhart et al., 2009), prostate cancer (Smith et al., 2004), and acromegaly (Dimaraki et al., 2004). The present findings show that raloxifene reduces visual deficits and visual system injury after focal cranial blast TBI in mice. Although the doses we used here are 5–10-fold higher than that used to treat osteoporosis and cancer in humans, the higher doses are also known to be safe in humans (Draper et al., 1996). Moreover, according to the FDA filing for raloxifene (Evista), no mortality was seen after a single oral dose in rats or mice at 5000 mg/kg or in monkeys at 1000 mg/kg. It is additionally important to note that we have shown that SMM-189 is effective in reducing increased fearfulness and depression stemming from brain trauma in our mouse model of focal cranial blast TBI (Reiner et al., 2015; Bu et al., 2016), and our preliminary results suggest raloxifene has similar benefit in this model. Even mild TBI in humans commonly leads to persistent and psychologically debilitating symptoms that can include anxiety, fearfulness, and depression (Bombardier et al., 2010; Bazarian et al., 2013). In this regard then, a regimen of raloxifene delivered in the aftermath of head trauma may also help reduce the adverse psychological outcomes from TBI in humans.

An important consideration for treating TBI in humans is when treatment must be begun and how long it must be continued. Consistent with the peak pro-inflammatory behavior of microglia in left retina and optic nerve during the first 3 days after injury, we found that treatment must be initiated no later than day 3 for maximum benefit. Microglial activation in the right eye and optic nerve appears to develop more slowly, and at least some right eye deficits could be rescued even with treatment begun at 3 days. We do not know if a full two weeks of treatment is needed for full benefit and, while the higher dose generally appears more effective, further work is required to optimize dosage. Taken together our findings that raloxifene rescues functional deficits and pathological changes following TBI in our mouse model support further consideration of raloxifene as a TBI therapy. With its FDA approval as safe for humans, a phase 2 clinical trial could start at any time, and if found effective, raloxifene could be repurposed for human use relatively quickly.

5. Conclusions

We found that 5–10 mg/kg raloxifene delivered daily for two weeks after blast mitigates or eliminates visual deficits that would otherwise be exhibited and decreases retinal, optic nerve, and oculomotor nucleus pathology, with the higher dose generally more effective. This rescue with raloxifene appears attributable to its CB2 inverse agonism and is accompanied by a biasing of microglia from the harmful M1 to the helpful M2 state. Raloxifene treatment is still effective even when delayed until 48 h after TBI. Our studies provide a strong basis for phase-2 testing of raloxifene efficacy in reducing TBI deficits and pathology.

Declaration of Competing Interest

None.

Acknowledgements

Special thanks to Marion Joni, Conor Dorian, and Dr. Natalie Guley for technical assistance. The research was supported by The Methodist Hospitals Endowed Professorship in Neuroscience (AR), UTHSC Neuroscience Institute (CL), NIH Medical Student Research Fellowship Program at UTHSC (JBD & JHD), and DoD grant W81XWH-16-1-0076 (AR, MGH).

Appendix A. Supplementary data

Supplementary data to this article can be found online at https://

doi.org/10.1016/j.expneurol.2019.113063.

References

Armstrong, R.A., 2018. Visual problems associated with traumatic brain injury. Clin. Exp. Optom. 101, 716–726.

Ashton, J.C., Glass, M., 2007. The cannabinoid CB2 receptor as a target for inflammation-dependent neurodegeneration. Curr. Neuropharmacol. 5, 73–80.

Atwood, B.K., Straiker, A., Mackie, K., 2012. CB_2: therapeutic target-in-waiting. Prog. Neuro-Psychopharmacol. Biol. Psychiatry 38, 16–20.

Baver, S.B., Pickard, G.E., Sollars, P.J., Pickard, G.E., 2008. Two types of melanopsin retinal ganglion cell differentially innervate the hypothalamic suprachiasmatic nucleus and the olivary pretectal nucleus. Eur. J. Neurosci. 27, 1763–1770.

Bazarian, J.J., Donnelly, K., Peterson, D.R., Warner, G.C., Zhu, T., Zhong, J., 2013. The relation between posttraumatic stress disorder and mild traumatic brain injury acquired during operations enduring freedom and Iraqi freedom. J. Head Trauma Rehabil. (1), 1–12.

Benedetto, M.M., Guido, M.E., Contin, M.A., 2017. Non-visual photopigments effects of constant light-emitting diode light exposure on the inner retina of Wistar rats. Front. Neurol. 8, 417.

Berson, D.M., Castrucci, A.M., Provencio, I., 2010. Morphology and mosaics of melanopsin-expressing retinal ganglion cell types in mice. J. Comp. Neurol. 518 (13), 2405–2422.

Bombardier, C.H., Fann, J.R., Temkin, N.R., Esselman, P.C., Barber, J., Dikmen, S.S., 2010. Rates of major depressive disorder and clinical outcomes following traumatic brain injury. JAMA 303 (19), 1938–1945.

Boudard, D.L., Mendoza, J., Hicks, D., 2009. Loss of photic entrainment at low illuminances in rats with acute photoreceptor degeneration. Eur. J. Neurosci. 30, 1527–1536.

Bricker-Anthony, C., Rex, T.S., 2015. Neurodegeneration and vision loss after mild blunt trauma in the C57Bl/6 and DBA/2J mouse. PLoS One 10 (7), e0131921.

Bricker-Anthony, C., Hines-Beard, J., Rex, T.S., 2014. Molecular changes and vision loss in a mouse model of closed-globe blast trauma. Invest. Ophthalmol. Vis. Sci. 55 (8), 4853–4862.

Bricker-Anthony, C., D'Surney, L., Lunn, B., Hines-Beard, J., Jo, M., Bernardo-Colon, A., Rex, T.S., 2017. Erythropoietin either prevents or exacerbates retinal damage from eye trauma depending on treatment timing. Optom. Vis. Sci. 94 (1), 20–32.

Bruce, B.B., Zhang, X., Kedar, S., Newman, N.J., Biousse, V., 2006. Traumatic homonymous hemianopia. J. Neurol. Neurosurg. Psychiatry 77, 986–988.

Bu, W., Ren, H., Deng, Y., Del Mar, N., Guley, N., Moore, B., Honig, M.G., Reiner, A., 2016. Mild traumatic brain injury produces neuron loss that can be rescued by modulating microglial activation using a CB2 receptor inverse agonist. Front. Neurosci. 10, 449.

Caeyenberghs, K., Leemans, A., Geurts, M., Taymans, T., Vander Linden, C., Smits-Engelsman, B.C., Sunaert, S., Swinnen, S.P., 2010. Brain-behavior relationships in young traumatic brain injury patients: fractional anisotropy measures are highly correlated with dynamic visuomotor tracking performance. Neuropsychologia 48, 1472–1482.

Capó-Aponte, J.E., Jorgensen-Wagers, K.L., Sosa, J.A., Walsh, D.V., Goodrich, G.L., Temme, L.A., Riggs, D.W., 2017. Visual dysfunctions at different stages after blast and non-blast mild traumatic brain injury. Optom. Vis. Sci. 94 (1), 7–15.

Collison, F.T., Park, J.C., Fishman, G.A., McAnany, J.J., Stone, E.M., 2015. Full-field pupillary light responses, luminance thresholds, and light discomfort thresholds in CEP290 Leber congenital amaurosis patients. Invest. Ophthalmol. Vis. Sci. 56, 7130–7136.

Deng, Y.P., Reiner, A., 2016. Cholinergic interneurons in the Q140 knockin mouse model of Huntington's disease: reductions in dendritic branching and thalamostriatal input. J. Comp. Neurol. 524 (17), 3518–3529.

Dimaraki, E.V., Symons, K.V., Barkan, A.L., 2004. Raloxifene decreases serum IGF-I in male patients with active acromegaly. Eur. J. Endocrinol. 150, 481–487.

Dobolyi, A., Vincze, C., Pál, G., Lovas, G., 2012. The neuroprotective functions of transforming growth factor beta proteins. Int. J. Mol. Sci. 13 (7), 8219–8258.

Donat, C.K., Fischer, F., Walter, B., Deuther-Conrad, W., Brodhun, M., Bauer, R., Brust, P., 2014. Early increase of cannabinoid receptor density after experimental traumatic brain injury in the newborn piglet. Acta Neurobiol. Exp. 74, 197–210.

Donat, C.K., Scott, G., Gentleman, S.M., Sastre, M., 2017. Microglial activation in traumatic brain injury. Front. Aging Neurosci. 9, 208.

Doyle, K.P., Cekanaviciute, E., Mamer, L.E., Buckwalter, M.S., 2010. TGFβ signaling in the brain increases with aging and signals to astrocytes and innate immune cells in the weeks after stroke. J. Neuroinflammation 7, 62.

Draper, M.W., Flowers, D.E., Huster, W.J., Neild, J.A., Harper, K.D., Arnaud, C., 1996. A controlled trial of raloxifene (LY139481) HCl: impact on bone turnover and serum lipid profile in healthy postmenopausal women. J. Bone Miner. Res. 11, 835–842.

Du, T., Ciuffreda, K.J., Kapoor, N., 2005. Elevated dark adaptation thresholds in traumatic brain injury. Brain Inj. 19, 1125–1138.

Fernández-Arjona, M.M., Grondona, J.M., Granados-Durán, P., Fernández-Llebrez, P., López-Ávalos, M.D., 2017. Microglia morphological categorization in a rat model of neuroinflammation by hierarchical cluster and principal components analysis. Front. Cell. Neurosci. 11, 235.

Franco, R., Fernández-Suárez, D., 2015. Alternatively activated microglia and macrophages in the central nervous system. Prog. Neurobiol. 131, 65–86.

Frick, K.M., Kim, J., Tuscher, J.J., Fortress, A.M., 2015. Sex steroid hormones matter for learning and memory: estrogenic regulation of hippocampal function in male and female rodents. Learn. Mem. 22, 472–493.

Goodrich, G.L., Flyg, H.M., Kirby, J.E., Chang, C.Y., Martinsen, G.L., 2013. Mechanisms of TBI and visual consequences in military and veteran populations. Optom. Vis. Sci. 90, 105–112.

Guley, N.H., Rogers, J., Del Mar, N., Deng, Y., Islam, R.M., D'Surney, L., Ferrell, J., Deng, B., Hines-Beard, J., Bu, W., Ren, H., Elberger, A.J., Marchetta, J., Rex, T.S., Honig, M.G., Reiner, A., 2016. A novel closed-head model of mild traumatic brain injury using focal primary overpressure blast to the cranium in mice. J. Neurotrauma 33, 403–422.

Guley, N.M., Del Mar, N.A., Ragsdale, T., Li, C., Perry, A.M., Moore, B.M., Honig, M.G., Reiner, A., 2019. Amelioration of visual deficits and visual system pathology after mild TBI with the cannabinoid type-2 receptor inverse agonist SMM-189. Exp. Eye Res. 182, 109–124.

Habib, P., Beyer, C., 2015. Regulation of brain microglia by female gonadal steroids. J. Steroid Biochem. Mol. Biol. 146 (3–14).

Hanisch, U.K., 2013. Functional diversity of microglia - how heterogeneous are they to begin with? Front. Cell. Neurosci. 7, 65.

Heldt, S.A., Elberger, A.J., Deng, Y., Guley, N.H., Del Mar, N., Rogers, J., Choi, G.W., Ferrell, J., Rex, T.S., Honig, M.G., Reiner, A., 2014. A novel closed-head model of mild traumatic brain injury caused by primary overpressure blast to the cranium produces sustained emotional deficits in mice. Front. Neurol. 5, 2.

Hines-Beard, J., Marchetta, J., Gordon, S., Chaum, E., Geisert, E.E., Rex, T.S., 2012. A mouse model of ocular blast injury that induces closed globe anterior and posterior pole damage. Exp. Eye Res. 99, 63–70.

Hiploylee, C., Dufort, P.A., Davis, H.S., Wennberg, R.A., Tartaglia, M.C., Mikulis, D., Hazrati, L.N., Tator, C.H., 2017. Longitudinal study of postconcussion syndrome: not everyone recovers. J. Neurotrauma 34 (8), 1511–1523.

Hughes, S., Watson, T.S., Foster, R.G., Peirson, S.N., Hankins, M.W., 2013. Nonuniform distribution and spectral tuning of photosensitive retinal ganglion cells of the mouse retina. Curr. Biol. 23, 1696–1701.

Jacobs, S.M., Van Stavern, G.P., 2013. Neuro-ophthalmic deficits after head trauma. Curr. Neurol. Neurosci. Rep. 13 (11), 389.

Jha, M.K., Lee, W.H., Suk, K., 2016. Functional polarization of neuroglia: implications in neuroinflammation and neurological disorders. Biochem. Pharmacol. 103, 1–16.

Kumar, A., Loane, D.J., 2012. Neuroinflammation after traumatic brain injury: opportunities for therapeutic intervention. Brain Behav. Immun. 26 (8) 1191–20.

Kumar, P., Song, Z.H., 2013. Identification of raloxifene as a novel CB2 inverse agonist. Biochem. Biophys. Res. Commun. 435, 76–81.

Kumar, A., Alvarez-Croda, D.M., Stoica, B.A., Faden, A.I., Loane, D.J., 2016. Microglial/macrophage polarization dynamics following traumatic brain injury. J. Neurotrauma 33 (19), 1732–1750.

Lachapelle, J., Ouimet, C., Bach, M., Ptito, A., McKerral, M., 2004. Texture segregation in traumatic brain injury – a VEP study. Vis. Res. 44, 2835–2842.

Lawrence, T., Natoli, G., 2011. Transcriptional regulation of macrophage polarization: enabling diversity with identity. Nat. Rev. Immunol. 11, 750–761.

Li, X.M., Yang, Q., Li, X.B., Cheng, Q., Zhang, K., Han, J., Zhao, J.N., Liu, G., Zhao, M.G., 2017. Estrogen-like neuroprotection of isopsoralen against spinal cord injury through estrogen receptor ERα. Metab. Brain Dis. 32 (1), 259–265.

Lin, B., Peng, E.B., 2013. Retinal ganglion cells are resistant to photoreceptor loss in retinal degeneration. PLoS One 8 (6), e68084.

Liu, Y., McAfee, S.S., Guley, N.M., Del Mar, N., Bu, W., Heldt, S.A., Honig, M.G., Moore 2nd, B.M., Reiner, A., Heck, D.H., 2017. Abnormalities in dynamic brain activity caused by mild traumatic brain injury are partially rescued by the cannabinoid type-2 receptor inverse agonist SMM-189. eNeuro.18 4 (4).

Loane, D.J., Kumar, A., 2016. Microglia in the TBI brain: the good, the bad, and the dysregulated. Exp. Neurol. 275 Pt 3, 316–327.

Lunn, C., Fine, J., Rojas-Triana, A., Jackson, J., Fan, X.D., Kung, T., Gonsiorek, W., Schwarz, M., Lavey, B., Kozlowski, J., Narula, S., Lundell, D., Hipkin, R., Bober, L., 2006. A novel cannabinoid peripheral cannabinoid receptor-selective inverse agonist blocks leukocyte recruitment in vivo. J. Pharmacol. Exp. Ther. 316, 780–788.

Lunn, C., Reich, E.-P., Fine, J., Lavey, B., Kozlowski, J., Hipkin, R., Lundell, D., Bober, L., 2008. Biology and therapeutic potential of cannabinoid CB2 receptor inverse agonists. Br. J. Pharmacol. 153, 226–239.

Madathil, S.K., Wilfred, B.S., Urankar, S.E., Yang, W., Leung, L.Y., Gilsdorf, J.S., Shear, D.A., 2018. Early microglial activation following closed-head concussive injury is dominated by pro-inflammatory M-1 type. Front. Neurol. 9, 964.

Magid, L., Heymann, S., Elgali, M., Avram, L., Cohen, Y., Liraz-Zaltsman, S., Mechoulam, R., Shohami, E., 2019. Role of CB2 receptor in the recovery of mice after traumatic brain injury. J. Neurotrauma. https://doi.org/10.1089/neu.2018.6063. (Epub ahead of print).

Matynia, A., Parikh, S., Chen, B., Kim, P., McNeill, D.S., Nusinowitz, S., Evans, C., Gorin, M.B., 2012. Intrinsically photosensitive retinal ganglion cells are the primary but not exclusive circuit for light aversion. Exp. Eye Res. 105, 60–69.

Matynia, A., Parikh, A., Deot, N., Wong, A., Kim, P., Nusinowitz, S., Gorin, M.B., 2015. Light aversion and corneal mechanical sensitivity are altered by intrinscally photosensitive retinal ganglion cells in a mouse model of corneal surface damage. Exp. Eye Res. 137, 57–62.

Matynia, A., Nguyen, E., Sun, X., Blixt, F.W., Parikh, S., Kessler, J., Pérez de Sevilla Müller, L., Habib, S., Kim, P., Wang, Z.Z., Rodriguez, A., Charles, A., Nusinowitz, S., Edvinsson, L., Barnes, S., Brecha, N.C., Gorin, M.B., 2016. Peripheral sensory neurons expressing melanopsin respond to light. Front. Neural Circuits 10, 60.

Morganti, J.M., Riparip, L.-K., Rosi, S., 2016. Call off the dog(ma): M1/M2 polarization is concurrent following traumatic brain injury. PLoS One 11 (1), e0148001.

Ouk, K., Hughes, S., Pothecary, C.A., Pierson, S.N., Morton, J.A., 2016. Attenuated pupillary light responses and downregulation of opsin expression parallel decline in circadian disruption in two different mouse models of Huntington's disease. Human. Mol. Gen. 25, 5418–5432.

Pisani, S.L., Neese, S.L., Katzenellenbogen, J.A., Schantz, S.L., Korol, D.L., 2016. Estrogen

receptor-selective agonists modulate learning in female rats in a dose- and task-specific manner. Endocrinology 157 (1), 292–303.
Presley, C., Abidi, A., Suryawanshi, S., Mustafa, S., Meibohm, B., Moore, B.M., 2015. Preclinical evaluation of SMM-189, a cannabinoid receptor-2 specific inverse agonist. Pharmacol. Res. Perspect. 3, e00159.
Raloxifene FDA Drug Approval Package, 1999. https://www.accessdata.fda.gov/drugsatfda_docs/nda/99/20815S3_Evista.cfm.
Reiner, A., Heldt, S.A., Presley, C.S., Guley, N.H., Elberger, A.J., Deng, Y., D'Surney, L., Rogers, J.T., Ferrell, J., Bu, W., Del Mar, N., Honig, M.G., Gurley, S.N., Moore, B.M., 2015. Motor, visual and emotional deficits in mice after closed-head mild traumatic brain injury are alleviated by the novel CB2 inverse agonist SMM-189. Int. J. Mol. Sci. 16, 758–787.
Schmidt, T.M., Chen, S.K., Hattar, S., 2011. Intrinsically photosensitive retinal ganglion cells: many subtypes, diverse functions. Trends Neurosci. 34, 572–580.
Schomberg, D., Olson, J., 2012. Immune responses of microglia in the spinal cord: contribution to pain states. Exp. Neurol. 234, 262–270.
Smith, M.R., Fallon, M.A., Lee, H., Finkelstein, J.S., 2004. Raloxifene to prevent gonadotropin-releasing hormone agonist-induced bone loss in men with prostate cancer: a randomized controlled trial. J. Clin. Endocrinol. Metab. 89, 3841–3846.
Stella, N., 2010. Cannabinoid and cannabinoid-like receptors in microglia, astrocytes and astrocytomas. Glia 58, 1017–1030.
Uebelhart, B., Herrmann, F., Rizzoli, R., 2009. Effects of the SERM raloxifene on calcium and phosphate metabolism in healthy middle-aged men. Clin. Cases. Miner. Bone. Metab. 6, 163–168.
Vest, V., Bernardo-Colón, A., Watkins, D., Kim, B., Rex, T.S., 2019. Rapid exposure to subthreshold trauma causes synergistic axonal damage and functional deficits in the visual pathway in a mouse model. J. Neurotrauma 36, 1646–1654.
Waters, E.M., Mitterling, K., Spencer, J.L., Mazid, S., McEwen, B.S., Milner, T.A., 2009. Estrogen receptor alpha and beta specific agonists regulate expression of synaptic proteins in rat hippocampus. Brain Res. 1290, 1–11.